J. Fluid Mech. (1994), vol. 279, pp. 279–311

Turbulent mixing in stratified fluids: layer formation and energetics

By YOUNG-GYU PARK[1] J. A. WHITEHEAD[2] AND ANAND GNANADESKIAN[1]

[1]MIT-WHOI Joint Program in Oceanography

[2]Department of Physical Oceanography

Woods Hole Oceanographic Institution, Woods Hole, MA 02543, USA

(Received 18 August 1993 and in revised form 27 May 1994)

Water with constant initial salt stratification was mixed with a horizontally moving vertical rod. The initially linear density profile turned into a series of steps when mixing was weak, in agreement with instability theory by Phillips (1972) and Posmentier (1977). For stronger mixing no steps formed. However, in all cases mixed layers formed next to the top and bottom boundaries and expanded into the interior due to the no-flux condition at the horizontal boundaries. The critical Richardson number Ri_c, dividing experiments with steps and ones without, increases with Reynolds number Re as $Ri_c \approx \exp(Re/900)$. Steps evolved over time, with small ones forming first and larger ones appearing later. The interior seemed to reach an *equilibrium state* with a collection of stationary steps. The boundary mixed layers continued to penetrate into the interior. They finally formed two mixed layers separated by a step, and ultimately acquired the same densities so the fluid became homogeneous. The length scale of the equilibrium steps, l_s, is a linear function of U/N_i, where U is the speed of the stirring rod and N_i is the buoyancy frequency of the initial stratification. The mixing efficiency R_f also evolved in relation to the evolution of the density structure. During the initiation of the steps, R_f showed two completely different modes of evolution depending on the overall Richardson number of the initial state, Ri_o. For $Ri_o \gg Ri_c$, R_f increased initially. However for Ri_o near Ri_c, R_f decreased. Then the steps reached an equilibrium state where R_f was constant at a value that depended on the initial stratification. The density flux was measured to be uniform in the layered interior irrespective of the interior density gradient during the equilibrium state. Thus, the density (salt) was transported from the bottom boundary mixed layer through the layered interior to the top boundary mixed layer without changing the interior density structure. The relationship between Ri_l and R_f was found for $Ri_l > 1$, where Ri_l is the Richardson number based on the thickness of the interface between the mixed layers. R_f decreases as Ri_l increases, consistent with the most crucial assumption of the instability theory of Phillips/Posmentier.

1. Introduction

One of the most difficult problems in oceanography and metcorology today is the specification of mixing and turbulent transport in stratified regions. The oceans and atmosphere contain motion that is described by a wide range of spatial and temporal scales. Many of these processes – internal waves, baroclinic instability, and double

diffusion to name a few – are thought to play important roles in the horizontal and vertical spreading of properties such as heat, moisture, dissolved tracers, momentum, vorticity and salt through the stratified oceans and atmosphere. In the oceans, mixing occurs throughout the stratified interior. In the atmosphere, although more attention has been focused on understanding the mixing in the unstratified troposphere, there are important consequences of mixing in the stratosphere. In the course of such studies, it has become clear that the interaction of the mixing with the stably stratified fluid nearby is an important process. Mixing in stratified fluids is also found in magma chambers, some industrial processes, and is also believed to be important in some stars.

Unfortunately, it remains difficult to directly measure the vertical flux of most quantities. Not only are vertical velocities difficult to measure in fluids that are for the most part stably stratified, but the correlation of that velocity with tracer fluctuations is more than doubly difficult to measure. As a result, oceanographers have tried to use observations of the mean temperature and velocity structure to infer the bulk properties of the mixing. In some cases (Munk 1966; Hogg *et al.* 1982; Whitehead & Worthington 1982), it was possible to use the mean temperature structure and some information about the mean vertical velocity to obtain basin-averaged estimates for vertical eddy diffusivities by using advective–diffusive balances. These techniques have yielded useful insights. However, they are at best an estimate of the effects of diffusivity, not a direct measurement of it.

Osborne & Cox (1972) proposed looking at the fine-scale temperature structure as a way of quantifying diffusivity. They developed a model in which the variance of the temperature gradient was essentially in a steady state, with variance being created in some locations by mixing events, and decaying in others. The intensity of mixing was parameterized as a ratio (the Cox number) between the gradient of fine structure and that of mean structure. Subsequent investigators (Gregg 1989, 1991; Schmitt *et al.* 1988) have used the fine-scale velocity structure to make estimates of the diffusive flux. Again, in these cases an assumption was made that turbulence is essentially in a statistically steady state, with a prescribed percentage of the energy input (about 84%) going to dissipation while the remainder goes to density transport.

Gibson (1980, 1982, 1986, 1987*a, b*) has criticized the diffusivities based on these measurements as being too small. He has advocated a picture of mixing in which energetic mixing events create packets of mixed fluid that then interleave with surrounding fluid to create temperature and salinity microstructure. It is his contention that microstructure profilers usually miss these energetic events, so they underestimate the dissipation and underestimate the eddy diffusivity.

Essentially, all of the above methods are inverse methods in the sense that for a given *signature* of mixing (temperature or velocity variance or mean structure), they attempted to reconstruct features of the mixing process itself. It seemed a useful exercise to the present authors to actually measure the density structure that would be produced by various intensities of mixing. In particular, we wanted to see if we could create interfaces and layers, i.e. steps, by stirring a fluid uniformly. Furthermore, we wanted to see if these steps would tell us anything about the energetics of the mixing process: the conversion of turbulent kinetic energy to mean potential energy.

1.1. *Theoretical background and previous experiments*

Phillips (1972) and Posmentier (1977) proposed similar hydrodynamic instability theories for step-like density structure formation. It was predicted that in the presence of turbulence, a linear density profile in a field of gravity is unstable to small

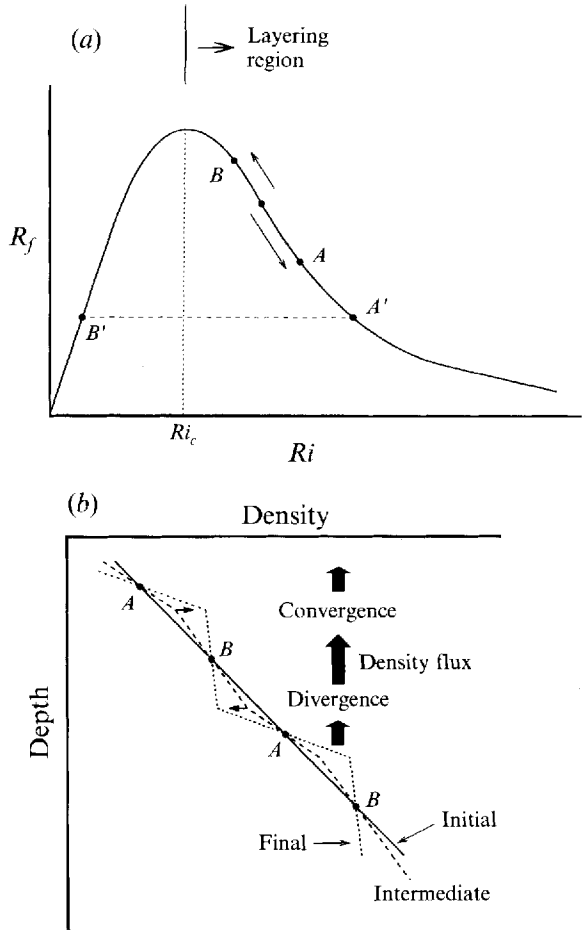

FIGURE 1. (*a*) The conceptual relation between the mixing efficiency, R_f, and a suitably defined Richardson number Ri. Layering is expected to the right of the point Ri_c, where R_f is maximum. (*b*) A schematic diagram of the evolution of density profile when $Ri_o > Ri_c$. At points A, Ri increases over time and the density flux decreases. At points B, Ri decreases over time and the density flux increases. A convergence of the density flux occurs at the top of negative perturbation to the gradient, but a divergence occurs at the bottom of it. The perturbation intensifies until the buoyancy flux becomes uniform throughout the region.

perturbations in the vertical density gradient if the stratification is strong compared to the intensity of the turbulence. The theory is based on a relation that is thought to relate the flux Richardson number or the mixing efficiency R_f (the ratio of change in potential energy caused by mixing to turbulent kinetic energy), and a suitably defined Richardson number Ri, which is basically the ratio of the potential energy stored in stratification to turbulent kinetic energy. In this relation, R_f increases from zero to a maximum as Ri goes from zero to a critical Richardson number Ri_c, and decreases as Ri increases beyond Ri_c as sketched in figure 1(*a*). The physical reason for R_f becoming small for $Ri \gg Ri_c$ is that the stratification is so strong that vertical velocity is inhibited. Three-dimensional turbulence is suppressed so it cannot mix the density field effectively. This relationship is verified in this experiment and discussed in § 4.2. In the other case, R_f becomes small for $Ri < Ri_c$ because there is not much density

gradient for the turbulence to mix. Hence, for $Ri \approx Ri_c$ the gradient is most efficiently mixed.

The stability theory assumes that there is homogeneous turbulence with constant vertical buoyancy flux throughout a uniform density gradient. Let the vertical density gradient be perturbed locally as illustrated in figure 1(*b*) so Ri is increased where the vertical density gradient is intensified (points labelled A, negative perturbation to the density gradient), and decreased where the density gradient is weakened (points labelled B, positive perturbation to the density gradient). There is a change in R_f in response to the change in Ri. For initial $Ri > Ri_c$, the positive density gradient perturbation locally increases the buoyancy flux, while the negative density gradient perturbation decreases it. Thus, buoyancy flux converges at the top of the region where the density gradient is weakened, and diverges at the bottom of the region (which is also the top of the region where the density gradient is intensified). This causes the perturbation to grow, which continues until point B moves to the left along the curve in figure 1(*a*) to the point B', and point A moves to the right to the point A'. The buoyancy flux across the layers and interface is in balance so that an *equilibrium state* is achieved. Posmentier (1977) showed that in the steady state, the buoyancy flux becomes a constant irrespective of the density gradient so point B' represents the layer and A' represents the interface between the layers. However, his theory cannot determine the constant except to indicate that the density flux of the equilibrium state is lower than that of the initial state.

In contrast to the above situation, if $Ri < Ri_c$ then divergence in density flux occurs at the top of the region where the density gradient is weakened, and convergence at the bottom of the region, so the perturbation decays. In their papers, Phillips (1972) used the relationship between buoyancy flux and vertical density gradient, and Posmentier (1977) used salt flux and the gradient of salt, instead of R_f and Ri. However, R_f and Ri are equivalent to a density flux and a density gradient, respectively. Posmentier (1977) calculated the evolution of the vertical salinity distribution numerically with an empirical relation between vertical eddy diffusivity, K, and Ri. Neither theory could predict the length scale of a layer. The stability equations were diffusion equations with negative diffusion coefficients or time-reversed diffusion equations, so the smallest scale grew most rapidly. This phenomenon is very unlikely in a real situation. Phillips (1972) suggested that the minimum length scale in nature should depend on the smallest scale over which the buoyancy flux can be regarded as a local function.

The most critical assumption of the Phillips/Posmentier theory is the dependence of R_f on Ri. Many laboratory experiments have been designed to measure this relationship. In most, two mixed layers of fluid were prepared and turbulence was introduced to either the upper or lower layer (Turner 1968; Linden 1979, 1980). The change in the density of each layer was measured so that the relationship between R_f and Ri was constructed. Linden (1979) combined previous experimental results with his own experiment to show the whole trend similar to figure 1(*a*). Owing to the difference between the mechanical mixers, each data set showed different maximum mixing efficiency. By dropping a horizontal grid across a density interface, Linden (1980) also shows the whole trend. Recently, Ivey & Imberger (1991) produced the relationship using an energetics argument along with the results of existing grid-generated turbulent mixing experiments in water and wind tunnels. To scale the data, the overturn Froude number was used instead of the Richardson number. The overturn Froude number is the square root of the inverse of the Richardson number based on turbulent length and velocity scales.

The above experiments have been useful in determining the mixing properties of fully developed layers, but may not be appropriate for describing the mixing properties of a uniformly stratified state. A few other experiments have focused on layer formation. Thorpe (1982) stirred linearly stratified fluid with laterally moving vertical grids and Ivey & Corcos (1982) did an experiment with a vertically moving rough plate. A series of turbulent mixed layers intruded into the non-turbulent ambient fluid away from the grid so that a step-like structure was generated outside the active turbulent region. According to the local instability theory, steps are formed within the turbulent region, so it is not difficult to conclude that the steps observed by Thorpe (1982) and Ivey & Corcos (1982) were associated with a somewhat different mechanism. For instance, Ivey & Corcos (1982) showed that the intrusive layer was due to the collapse of turbulent eddies in stratified surroundings. Since the intrusion made a negligible direct contribution to the vertical buoyancy flux, it could not satisfy one of the necessary conditions of the theory. Thorpe (1982) tried to relate the step-like structure to the instability theory, but could not verify the theory.

Ruddick, McDougall & Turner (1989) stirred salt- or sugar-stratified fluids with an array of vertical rods moved horizontally throughout the depth and length of a tank. A linear stratification turned into a series of steps when the stirring was weak, and the steps disappeared as the stirring became strong, as the theory of Phillips/Posmentier predicted. Until now, this is the only experiment that has examined the Phillips/Posmentier theory. Their experiment was pioneering but exploratory, with qualitative observation results over a small range of parameters. Many questions remain unanswered. Among them the most fundamental questions are *What does the stability boundary look like?*: *Is there a value of* Ri_c *and what governs it?*, *What are the energetics of layer formation?*, *What is the evolution of the layer formation?* This study is designed to quantitatively answer these questions.

Almost linearly salt-stratified fluids were stirred uniformly with vertical rods moved horizontally at constant speeds. The evolution of the density profiles was measured until the fluids were completely mixed using a conductivity probe with a spatial resolution of about 1 mm. It was possible to get accurate control of the rods' speed, and to calculate change in potential energy due to mixing. The energy budget was used to investigate the energetics of layering, focusing on the difference between the layering and non-layering cases. Since the fluids were mixed until they became almost homogeneous, it was possible to relate the mixing efficiency and density flux to the evolution of the density fields. An empirical relation between the size of the step and external parameters was documented. Finally, by changing the stratification and the speed of the stirring rods as widely as the apparatus allowed, the stability boundary for layer formation was documented.

In § 2, the design and procedure of the experiments are described. In § 3, the evolution of the density profiles depending on the parameters of the experiments is described, focusing on the evolution of layers and interfaces. The stability boundary is also discussed in this section. In § 4, the relation between the length scale of the steps and the external length scales of the experiments is discussed. The energetics of the layer formation are also discussed related to the evolution of the density structure. Finally, conclusions are in § 5.

2. The experiments

The objective of the experiments was to create turbulence by stirring a linearly stratified fluid with a rod, and to observe the evolution of the vertical density structure

after numerous stirring events. To characterize the energetics, it was necessary to calculate the kinetic energy input and the change in potential energy accurately. To meet the latter requirement, a conductivity probe was used to get density profiles of high spatial resolution. A linear motion system connected to programmable drivers was used to control the speed of the stirring rod.

The most important parameters of the experiments were the Reynolds number of the rod, Re, and the overall Richardson number, Ri_o, defined as

$$Re = \frac{UD}{\nu},$$

$$Ri_o = \frac{N_i^2 D^2}{U^2}.$$

Here, N_i is the buoyancy frequency of an initial stratification, U is the speed of the rod (which consequently is the speed of the turbulent eddies), ν is kinematic viscosity, and D is the diameter of the rod (consequently the diameter of the eddies). Other parameters are the Prandtl number, $Pr = \nu/\kappa_s$, and the Péclet number, $Pe = UD/\kappa_s$, where κ_s is the molecular diffusivity of salt. Only salt was used in preparing stratified fluids so that Pr was fixed throughout the experiments, and Pe was proportional to Re.

2.1. *Apparatus and procedure*

Using the Öster method, a 20 cm × 10 cm × 45 cm Plexiglas tank was filled with an almost linearly salt-stratified fluid. The initial stratification was measured with a conductivity probe at the beginning of every run. A vertical rod of diameter D was used as a stirrer with D being either 1.29, 2.26 or 3.33 cm. The tip of the rod was placed 0.5 cm above the bottom of the tank. The rod was connected to a sliding carriage driven by a stepper motor by means of a threaded rod. The stepper motor driver was controlled by a computer so that precise driving speeds could be specified. The rod moved back and forth a programmed distance at a constant speed throughout each run. One back and forth motion was defined as an *excursion*, and the length of one excursion was 28 cm in all runs. The speed of the rod varied between 1 and 7 cm s^{-1}. After repeating the excursion a predetermined number of times, the stirring rod was stopped for one or two minutes while energetic turbulence decayed. This was confirmed visually using a shadowgraph during some runs. Then, the conductivity probe was lowered by another stepper motor. A *cycle* that consisted with a sequence of stirring, waiting and profiling was repeated until the fluid was almost mixed. A schematic diagram of the experiment is shown in figure 2.

Since the conductivity data were used to get the density structure, the calibration of the probe was important. The probe is a Model 125 four-prong (two active and two passive) conductivity microprobe made by Precision Measurement Engineering. The conductivity profiles were converted to density profiles after a run. The probe has an effective sampling volume of 1 mm^3 and a time constant in the range of 10^{-3} s or faster. It was calibrated before each run with five samples of water. The density of the samples was measured directly with a densiometer (Anton Paar model DMA 46) precise to 10^{-4} g cm^{-3}. The probe was never taken out of the water throughout a run. The tip of the probe moved from 0.5 cm below the surface of the water to about 1 cm above the bottom at an average speed of 1 cm s^{-1}. During the downward motion the probe stopped at approximately every millimeter to measure conductivity, but the time required to make a reading was less than 0.01 s, so the speed of the probe movement was almost constant. A shadowgraph was also used to observe turbulence.

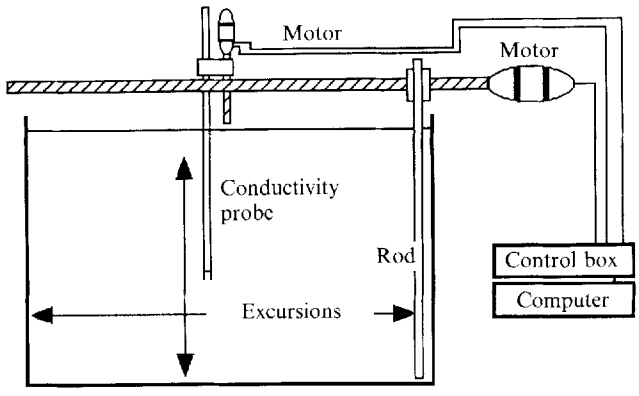

FIGURE 2. Schematic diagram of the experiment.

Time lapse movies and still pictures were taken during some runs. The screen for the shadowgraph was placed either at the wall or about 1 m in front of the tank to produce optimally focused images.

Since a temperature change could also cause some mixing, the temperature of the laboratory was kept constant. When a run took more than a day, the room temperature was recorded with a thermometer placed next to the tank. The variation in the room temperature was less than 2°C over a day. To avoid mixing due to the temperature difference between the laboratory and the test fluid, the fluid was placed in the laboratory more than 12 hours before the filling. At the time of filling the temperature difference between the room and the fluid was less than 1°C. Sideways heating can form layers of depth scale $l_t = \alpha \Delta T/(\partial\rho/\partial z)$ (Turner 1973). Here, α is the thermal expansion coefficient, ΔT is the temperature difference between the fluid and the room, and ρ is density. In the present experiments, l_t was less than 1 cm, which was smaller than the diameter of the smallest rod used. The tank was constructed of 0.95 cm thick Plexiglas to retard lateral heat transfer so that the effect of the temperature variation should not be significant.

The experiments were divided into two phases. The first phase focused on producing steps with turbulent mixing, and observing the evolution of density profiles. Several different stratifications were tested within a narrow range of Re variation. The present experiments showed formation of layers when the stratification was strong. This was in agreement with Ruddick *et al.* (1989). Three different sizes of rod were used to see if the size of the rod changed the step size. The second phase focused on finding the stability boundary of layer formation. Wide ranges of Re and Ri_o variations were produced within the limits of the apparatus. The change of Ri_o was obtained by changing both the stratification and the speed of the rod. The change of Re was obtained by varying the speed of the rod while D, the size of the rod, was fixed at 2.26 cm.

The parameters of all the 76 runs are listed in the Appendix. The runs are plotted in the (Ri_o, Re) parameter space as illustrated in figure 3. Ri_o was varied from around 0.2 to 12.3 and Re from 100 to 1600. Since keeping the speed of the stirring rod constant was easier than preparing exactly the same stratification for each run, the runs are aligned along a constant-Re line in the (Ri_o, Re) phase space.

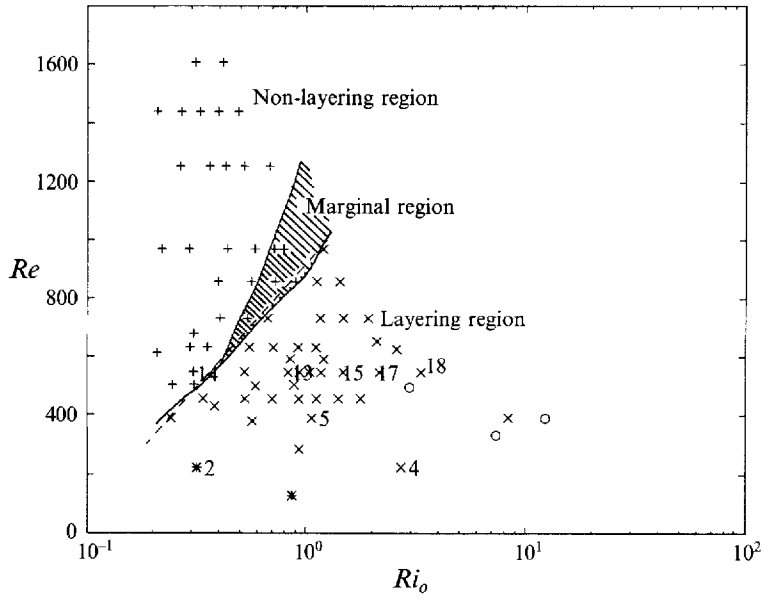

FIGURE 3. The stability curve and all the 76 runs in the (Ri_o, Re) space. Here, * is for the 1.29 cm diameter rod, × for the 2.26 cm rod, and o for the 3.33 cm rod. In the figure, the hatched region denotes the marginal region. The region below the hatched region is the unstable region (the layering region) and above is the stable region (the non-layering region). The boundary between the marginal region and the layering region is the stability boundary. The numbers in the figure denote run numbers shown in the following figures. The dashed line corresponds to the empirical relation given in (3.1).

2.2. *Data correction*

The raw density profile was processed before any calculations were made, even though it showed trends or characteristics clearly. First, density was linearly extrapolated to the top 5 mm and bottom 1 cm where the conductivity was not measured. Second, sometimes the probe generated noise spontaneously. This occurred in the later stages of some runs. The data were smoothed by applying a 9-point moving average. Third, the linear drift of the probe was corrected using mass conservation. The total mass of the fluid should be conserved during a run if the effect of evaporation is neglected. The evaporation was at most less than 1 mm/day. This caused less than 0.5% change in the mean density per day. To compensate for this minor change in density, all the density profiles of a run were shifted to give the same mean density.

3. Observations

3.1. *The evolution of the density profile and the stability boundary*

In every experiment, top and bottom boundary mixed layers developed before significant variations occurred in the interior. The no-flux condition across the top and bottom boundaries in the presence of diffusion required a vanishing vertical density gradient. Thus, the boundary mixed layers were produced there first, then they expanded into the interior over time. The interior, which is the focus of this study, showed different patterns of evolution depending on the external parameters Ri_o and Re.

For small Ri_o, the density profile showed two advancing boundary mixed layers

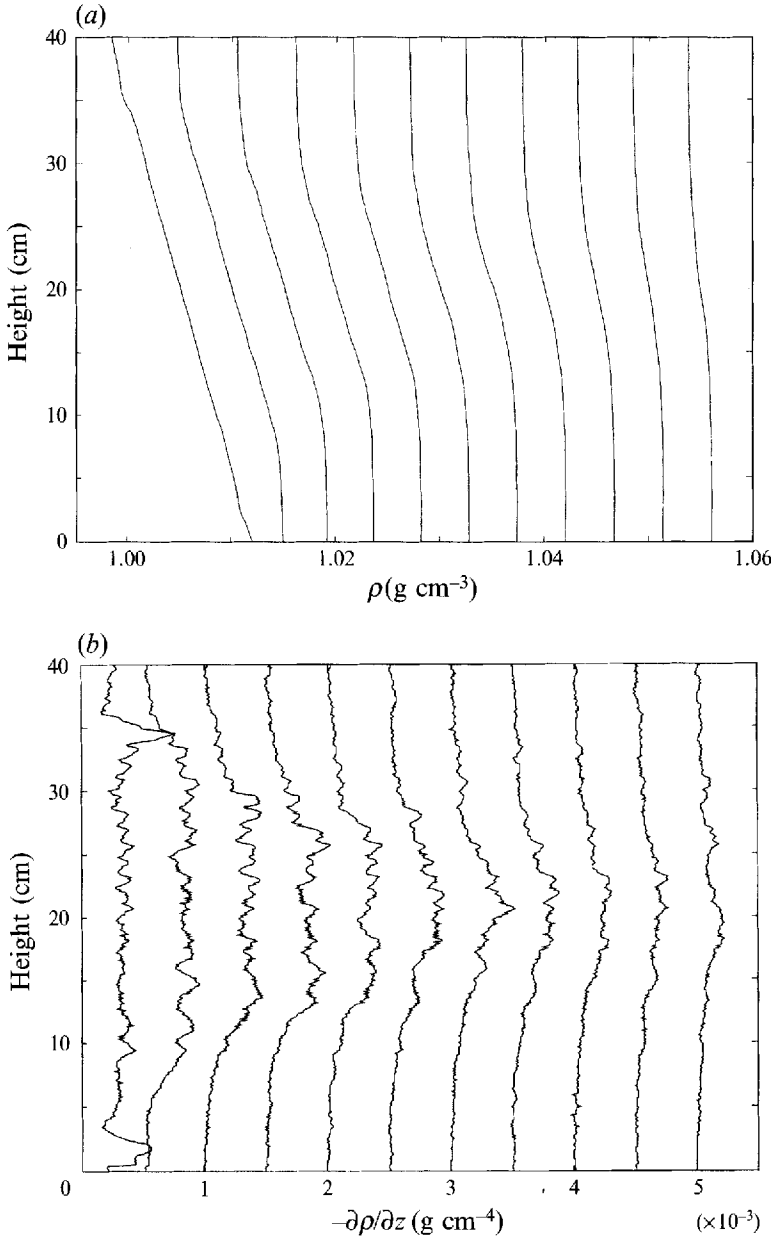

FIGURE 4. The evolution of the density field during Run 14. The values of Ri_o and Re of this run were 0.31 and 547, respectively, and they are above the stability curve in figure 3. (*a*) The density profile of the initial state and at every 60 excursions. Each plot is shifted by 0.005 g cm^{-3}. (*b*) The negative of the gradient of the density profiles in (*a*). Each plot is shifted by 0.0005 g cm^{-4}.

with an unchanging interior (see figures 4*a* and 4*b*). The density gradient shown in figure 4(*b*) is the first derivative obtained by the finite difference of the corrected density profile. The region between the boundary layers and the interior had no intensification of density gradient. The interior density gradient looked like a wide plateau in each profile with small scale *wiggles* of about 1.3 cm as shown in figure 4(*b*). (The wiggles were present from the beginning to the end of the run. They were

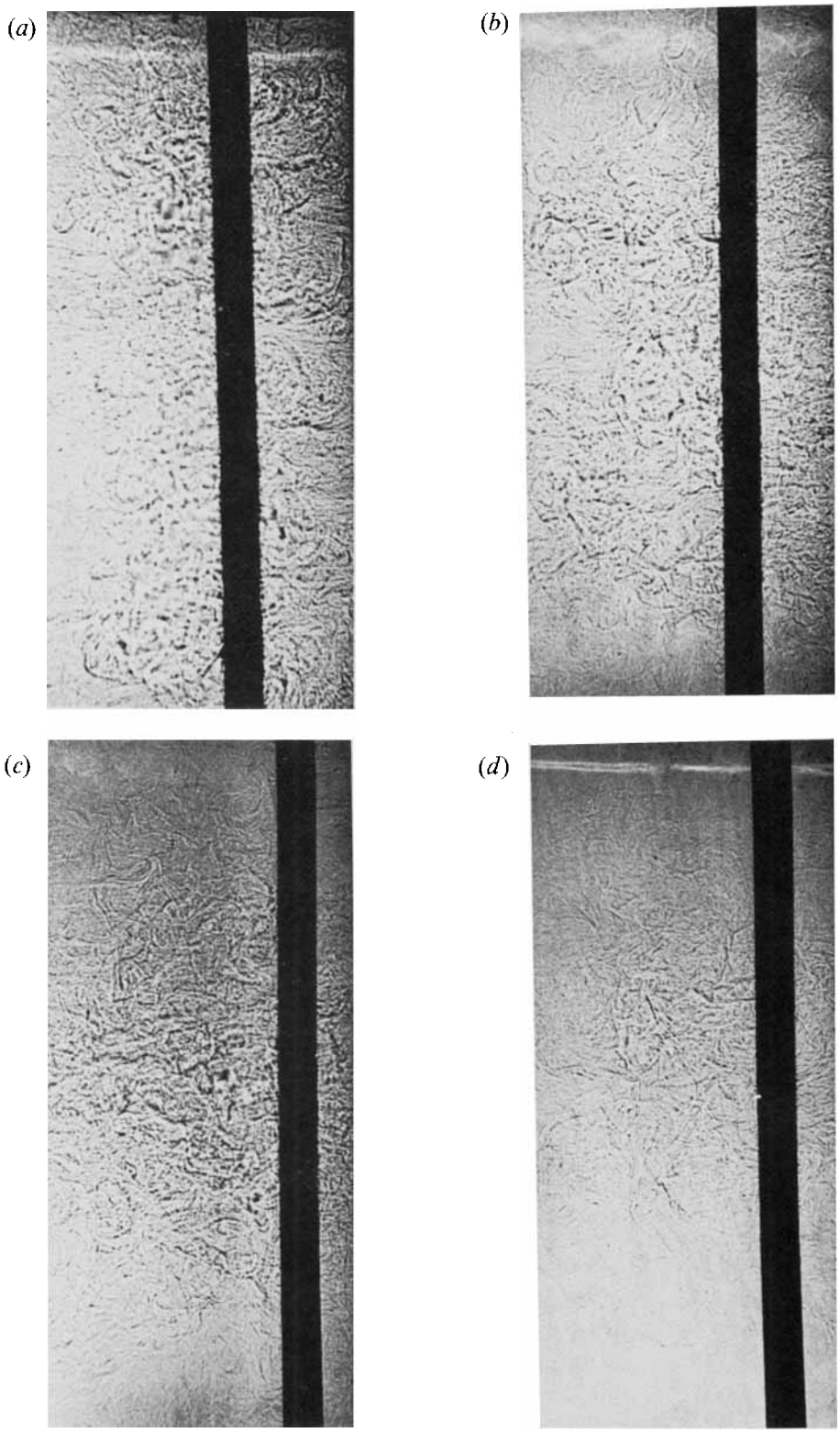

FIGURE 5 (*a–d*). For caption see facing page.

observed in many cases regardless of the external parameters but did not become amplified in any case. They were presumably due to turbulent fluctuations. Since the wiggle length scale was never amplified in any runs the presence of these small wiggles is henceforth neglected when explaining the structure of the interior.) As time progressed, the boundary mixed layers expanded to the interior monotonically so that the width of the plateau decreased. Figure 5 is a series of shadowgraphs taken during Run 14. The black vertical strip is the stirring rod of diameter 2.26 cm. No interface can be seen.

For a run with a larger Ri_o and roughly the same value of Re, interfaces formed first between the interior and boundary mixed layers (see figures 6*a* and 6*b*). The density gradient profile has two peaks, which represent interfaces between the mixed layers and the interior. The peaks were absent from the preceding density gradient profile (figure 4*b*). At first, these two interfaces intensified rapidly. Then they moved toward each other. At the same time the mean interior density gradient decreased slightly (see figure 6*b*). When the two interfaces became close enough, one of them became weaker and decayed; the fluid became two mixed layers with only one interface. The remaining interface also decayed over time and finally the fluid became homogeneous. (The small-scale wiggles were also observable during this run. The interfaces were about 5 cm thick and thicker than the wiggles, which were about 1.3 cm thick. Sometimes the wiggles overrode the interfaces but there was no difficulty in telling them apart.) Since this run showed the formation of two coherent interfaces† with one interior layer between the interfaces, and formation of interfaces was not observed during the runs with lower Ri_o such as Run 14, a transition point can be expected between the runs with these characteristics and the runs with lower Ri_o.

For a run with an even larger Ri_o and roughly the same Re, more interfaces and layers (steps) formed in the interior as illustrated in figures 7(*a*) and 7(*b*). The boundary mixed layers advanced rapidly after the beginning of mixing, and then the expansion rate slowed down as the interior structure was developing. After this time, the boundary layers did not continue to expand. Instead, the boundary layers showed sudden expansion into the interior along with the decay and merging of the outer interfaces. Figure 8 is a series of shadowgraphs taken during Run 17. The interfaces, which are white lines, were maintained under active turbulent mixing. (Thin white lines can be seen between the thick white lines. They are the small-scale wiggles of about 1.3 cm thick.)

For high enough Ri_o, the formation of steps that remained for some time without much change, as shown in figure 7, could be confirmed easily. However, for Ri_o near the stability boundary, steps that maintained their shape for some time were not observed. Step size increased as Ri_o came close to the stability boundary for fixed Re, as documented in § 4.1. Naturally, as the boundary layers expanded, the

† The coherent interfaces here may look different from those in the interior of some other runs, because the former moved to the interior but the latter did not. Considering the expansion of the boundary mixed layers, it was possible to trace the interfaces to the interior coherently.

FIGURE 5. A series of shadowgraphs taken during Run 14. The screen was placed about 1 m in front of the tank. Pictures were taken during (*a*) 5th excursion, (*b*) 111 st excursion, (*c*) 219 th excursion, and (*d*) 639 th excursion. The vertical black strip is the stirring rod with $D = 2.26$ cm. The signature of mixing becomes weaker over time. The signature of turbulent mixing is weak near the top and bottom boundaries.

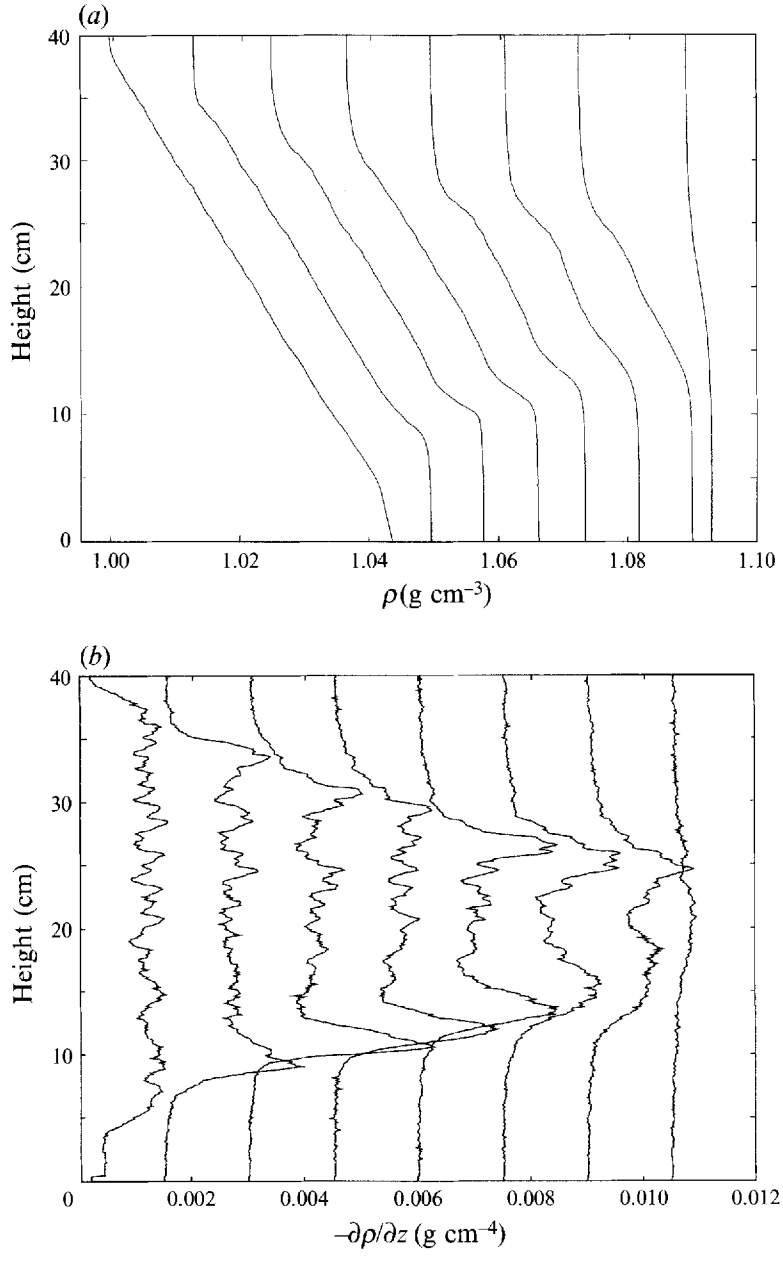

FIGURE 6. The evolution of the density field during Run 13. The values of Ri_ρ and Re of this run were 1.04 and 547, respectively, and they are slightly below the stability curve in figure 3. (*a*) The density profile of the initial state and after 150, 300, 450, 750, 950, 1150, and 2250 excursions. Each plot is shifted by 0.01 g cm^{-3}. (*b*) The negative of the gradient of the density profiles in (*a*). Each plot is shifted by 0.0015 g cm^{-4}. The interior mean density gradient slightly decreases over time.

interior shrinked. These factors made the determination of the stability boundary ambiguous at first. The evolution of a linear density profile to coherent interfaces while weakening the density gradient between the interfaces, as shown in figures 6(*b*) and 7(*b*), was defined as a *layering*. This is the clear proof of the Phillips/Posmentier instability theory, and used as an indicator of the instability.

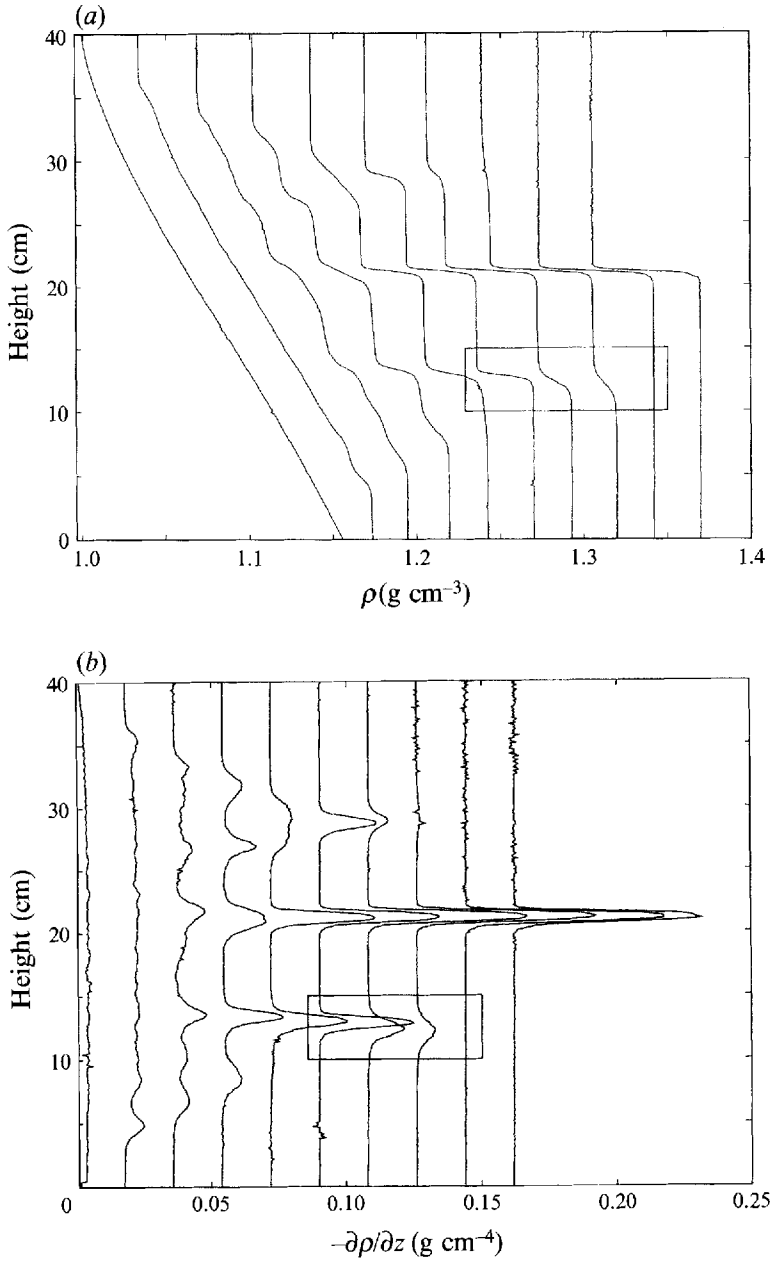

FIGURE 7. The evolution of the density field during Run 18. The values of Ri_o and Re of this run were 3.34 and 547, respectively, and they are far below the stability curve in figure 3. (*a*) The density profile of the initial state and after 300, 750, 1050, 1500, 1800, 2700, 3000, 3750, and 4500 excursions. Each plot is shifted by 0.01 g cm^{-3}. (*b*) The negative of the gradient of the density profiles in (*a*). Each plot is shifted by 0.02 g cm^{-4}. The boxes in the figures are examples of the decay of an interface. During the decay, the interface thickness increases.

The stability boundary, which is equivalent to Ri_c, was found by varying Ri_o and Re for individual runs as shown in figure 3. In the figure, the hatched region denotes a marginal region, where a transition from non-layering to layering occurs. The layering clearly happened below the marginal region. Above the marginal region the layering

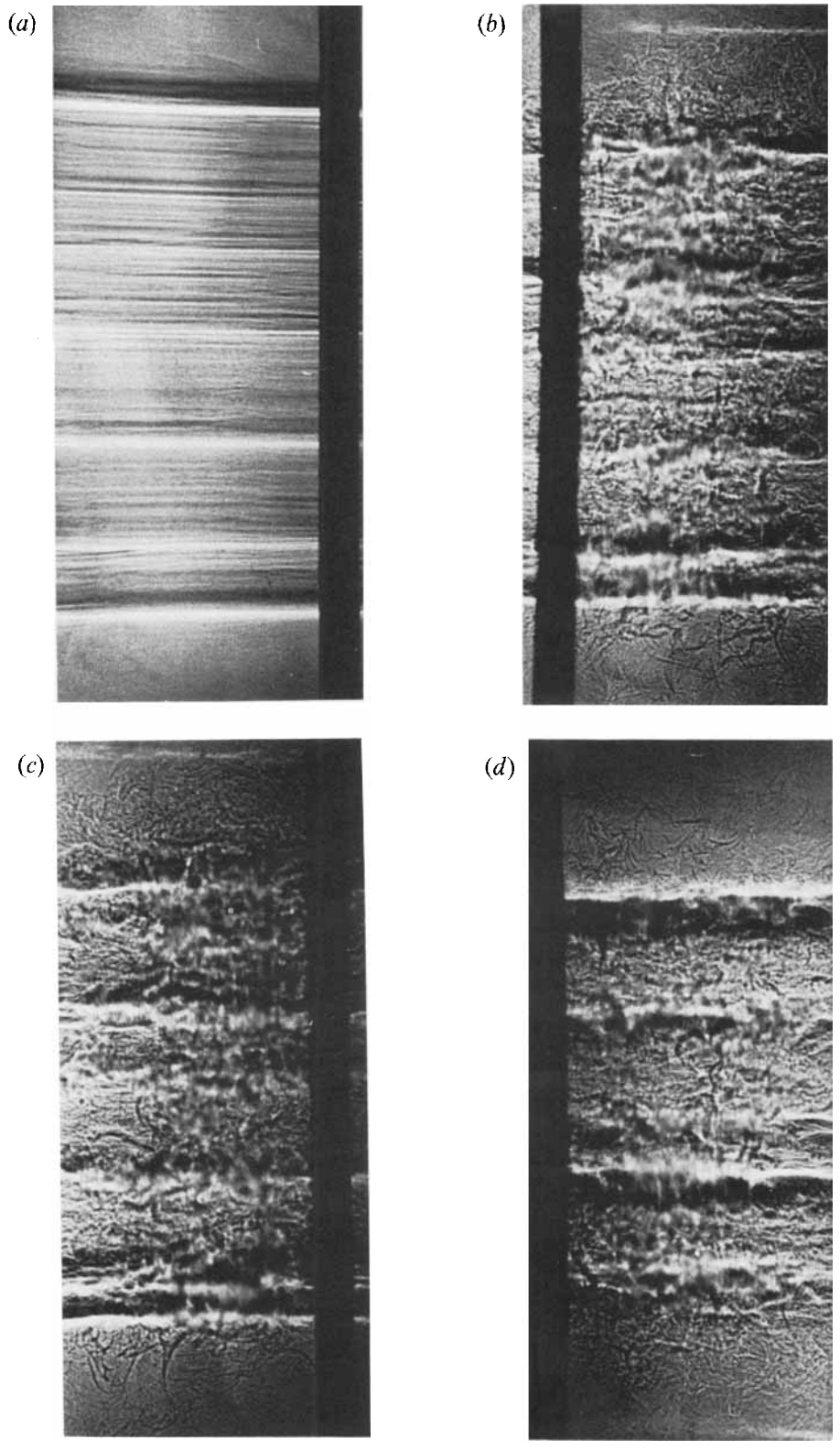

FIGURE 8 (*a–d*). For caption see facing page.

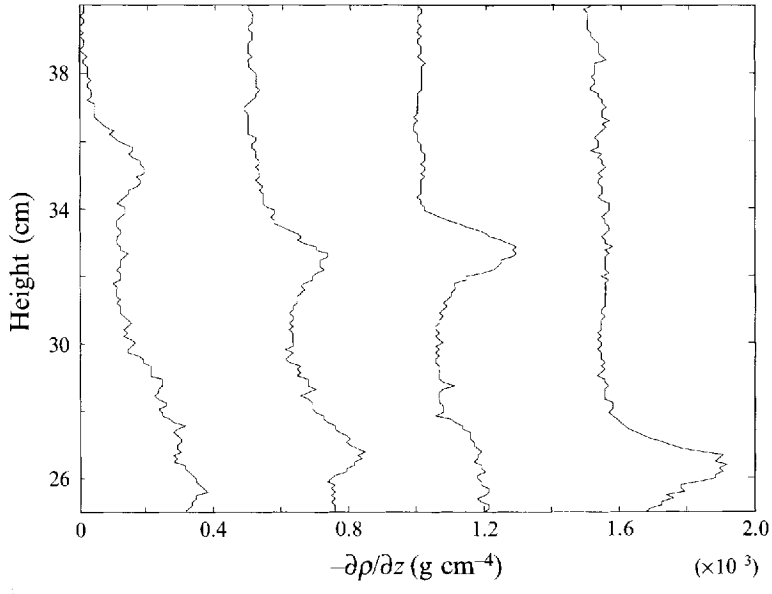

FIGURE 9. The profiles of the negative of the density gradient of Run 27. The values of Ri_o and Re of this run were 0.21 and 612, respectively, and they lie below the stability curve in figure 3. The profiles were taken after 100, 150, 200, 250 excursions. Each plot is shifted by 0.0005 g cm^{-3}. An interface forms at about 32 cm but then decays.

was not observed. In the non-layering region, transient interfaces that did not become intensified significantly beyond the initial stratifications and could not be traced for some time were occasionally observed. An example of such a transient interface is shown in figure 9. An interface formed at about 32 cm after 150 excursions but then decayed between the 200th and 250th excursion. The interface of the fourth plot of the figure also showed transient behaviour, though it is not plotted in the figure. In the marginal region, the evolution of the density field was not clear. The lower boundary of the marginal region was defined as our best estimate of the *stability boundary*, Ri_c. From these results the relationship between Ri_c and Re is

$$Ri_c \approx \exp(Re/900), \tag{3.1}$$

for $400 < Re < 1000$, and plotted in figure 3 as a dashed line.

When Ri_o was slightly larger than Ri_c, the difference between the layer and interfacial density gradients was small. Near Ri_c, R_f was high so that the boundary mixed layers expanded rapidly and might have overtaken the interior before interior layering became strong enough to be observed. Though the present experiments could not find Ri_c precisely and might have overestimated Richardson number of the stability boundary, the trend is clear. For high Re, owing to the rapid expansion of

FIGURE 8. A series of shadowgraphs taken during Run 17. The values of Ri_o and Re of this run were 2.15 and 547, respectively, and they are below the stability curve in figure 3. The screen was placed about 1 m in front of the tank. Pictures were taken during (*a*) 402nd excursion, (*b*) 582nd excursion, (*c*) 678th excursion, and (*d*) 800th excursion. The vertical black strip is the stirring rod with $D = 2.26$ cm. The two white strips near the bottom boundary come closer over time and finally become one. This is a visual example of the merging of interfaces.

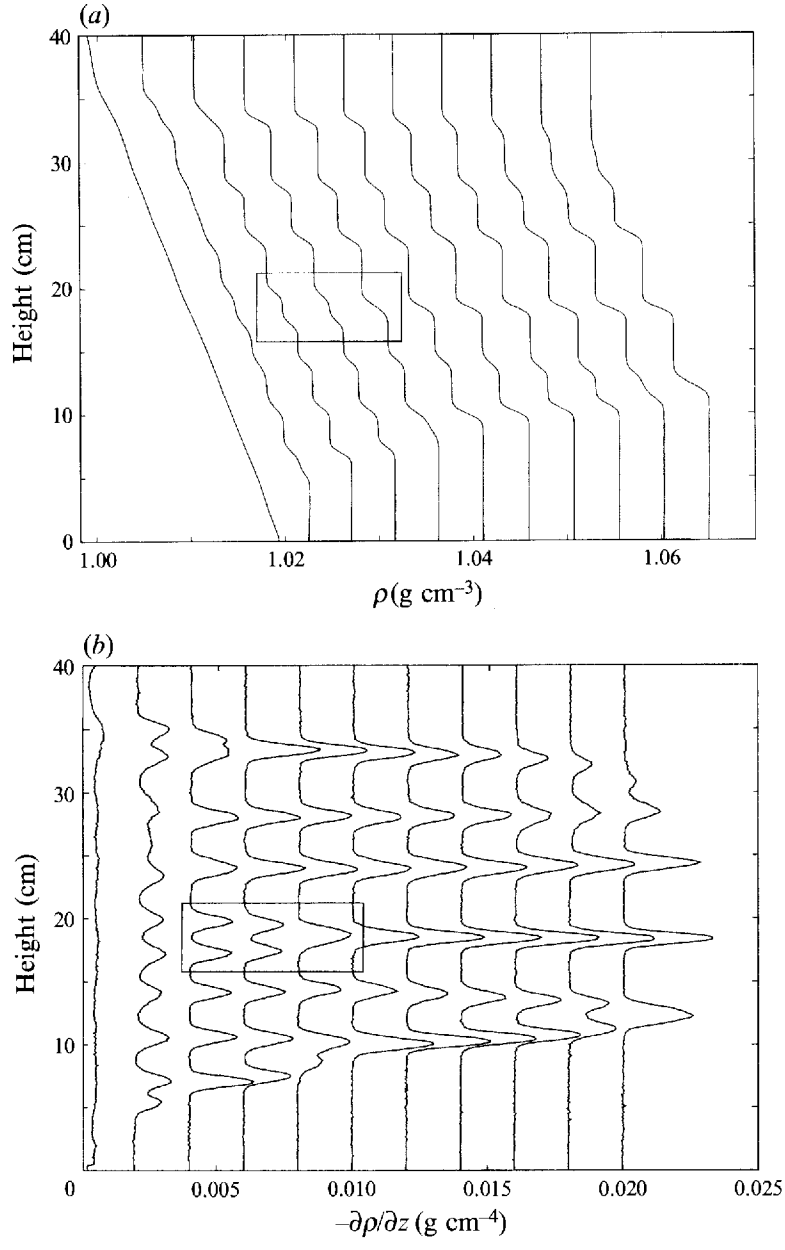

FIGURE 10. The evolution of the density field during Run 4. The values of Ri_o and Re of this run were 2.71 and 226, respectively, and they lie below the stability curve in Figure 3. (a) The density profile of the initial state and after every 300 excursions. Each plot is shifted by 0.0005 g cm^{-3}. (b) The negative of the gradient of the density profiles in (a). Each plot is shifted by 0.002 g cm^{-4}. The boxes in the figures are examples of the merging of interfaces.

the boundary mixed layers and high R_f, the marginal region expanded as illustrated in figure 3. For high Re, owing to the saturation of salt, it was not possible to achieve $Ri_o > Ri_c$. Thus, increasing Re beyond about 1000 while maintaining the same experimental set up was not useful.

3.2. *The evolution of the interior layer*

For the runs with $Ri_o > Ri_c$, turbulence broke down the uniform stratification into a series of steps. Figures 10(*a*) and 10(*b*) are sequences of the profiles of the density and density gradient taken during Run 4. The steps were in the form of periodic perturbations to the mean density gradient. Naturally, the height of the peaks in the density gradient profile increased as the density gradient of layers decreased and the density profile became a series of well-mixed layers with sharp density interfaces. Figures 10(*a*) and 10(*b*) clearly show the evolution of the interior steps. The sizes of steps increased through a merging or decay of interfaces. After some time, the merging or decay of interfaces usually occurred due to the advance of the boundary mixed layers, and the interior showed very little evolution. The interior seemed to reach an *equilibrium state* at this time. If there was no expansion of the boundary mixed layers then the interior was expected not to change. The boundary mixed layers, however, kept overtaking the interior and the number of steps decreased and the fluid eventually became homogeneous.

3.2.1. *The merging and the decay of interfaces*

The *decay* of interfaces was observed and explained by Ruddick *et al.* (1989). When the density differences across two adjacent interfaces are different, the density flux across the weak interface is larger according to the relationship between R_f and Ri_o. As a result, divergence occurs at the weak interface, causing eventual decay, while intensifying the adjacent interfaces. An example of the decay is shown in figure 11(*a*), which is a sequence of the density gradient profiles of Run 2. The interface in the middle is weaker than the adjacent ones that are above and below it. The middle interface decays over time, while the adjacent ones intensify. During the decay neither the thickness nor positions of the interfaces changed. In the interior, the decay was rarely observed. The expansion of the boundary layer was the main cause of the interface decay, and the small boxes in figures 7(*a*) and 7(*b*) are examples. During the decay caused by the expansion of the boundary mixed layers, the interface thickness increased. The decay of an interface was also observed at the ends of some runs. For runs with $Ri_o > Ri_c$, the fluid eventually turned into two mixed layers. As time progressed, the density jump across the interface, $\Delta\rho$, decreased slowly while the thickness of the interface remained almost constant. An example is shown in figure 11(*b*), which is a sequence of density gradient profiles taken during Run 18.

The *merging* of interfaces occurred when two interfaces were close, i.e. when a mixed layer was thin. The merging occurred even when the density differences across two adjacent interfaces were similar, so that a divergence of density flux could not happen. This implies that there is a minimum length scale for a layer, but the present experiments cannot verify such a length scale. In the interior, the merging occurred during the early stage of a run. During the merging, two interfaces and the layer between them became a new interface so the interfaces became thicker. Naturally, after the merging the length scale of the layer became larger and the new interface showed a larger density difference. The small boxes in figures 10(*a*) and 10(*b*) are good examples of such a merging. The expansion of the boundary mixed layers also caused the merging. Figure 8 gives a good visual example. The two white stripes near the bottom of the tank, which are interfaces, come close and eventually become one.

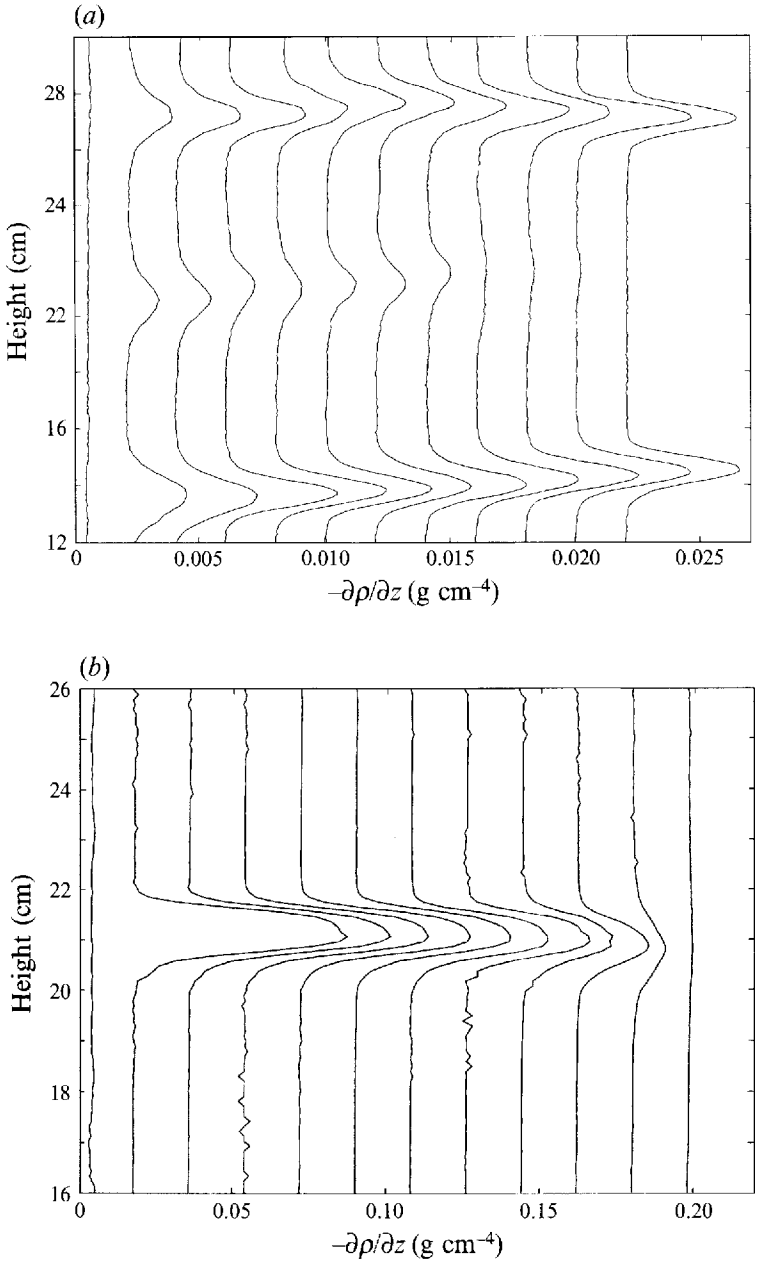

FIGURE 11. Examples of the decay of an interface. (*a*) The decay of an interior interface during Run 2. The values of Ri_o and Re of this run were 0.32 and 223, respectively, and they are below the stability curve in figure 3. Negative density gradient profiles are shown of the initial state, after 1000 excursions and for every 200 excursions thereafter. Each plot is shifted by 0.002 g cm^{-4}. (*b*) The decay of an interior interface during Run 18. Negative density gradient profiles are shown of the initial state, after 3000 excursions, and for every 750 excursions thereafter. Each plot is shifted by 0.018 g cm^{-4}. The thickness of the interface stays the same until almost the end of the run while the density difference across the interface gradually decreases.

Run number	Step size (cm)	U (cm s^{-1})	N_i (s^{-1})	U/N_i (cm)	D (cm)
2	6.6	1.70	0.74	2.29	1.29
4	3.2	1.00	0.73	1.37	2.26
5	6.9	1.70	0.77	2.19	2.26
7	3.2	1.00	0.81	1.23	3.33
9	3.4	1.60	1.68	0.95	3.33
10	3.7	2.77	1.96	1.41	2.26
11	4.0	1.73	2.21	0.78	2.26
15	6.2	2.42	1.30	1.86	2.26
16	7.6	2.42	1.16	2.09	2.26
17	5.5	2.42	1.57	1.54	2.26
18	5.3	2.42	1.96	1.24	2.26
19	4.7	2.02	1.19	1.70	2.26
21	7.1	2.02	0.94	2.14	2.26
22	6.5	2.02	1.06	1.91	2.26
23	6.6	2.02	0.86	2.35	2.26
26	8.8	1.67	0.56	3.00	2.26
28	5.3	1.26	0.54	2.34	2.26
54	5.8	3.24	1.98	1.63	2.26
76	8.7	2.42	1.03	2.34	2.26

TABLE 1. The sizes of the steps and the external parameters

4. Analysis

4.1. *The length scale of the steps*

Although the theory of Phillips/Posmentier did not predict any length scale of the steps, the density profiles such as those in figure 10(*a*) show the existence of one. To find what factors might determine the length scale of steps, the sizes of the steps were compared with the external length scales of the experiments, which were the diameter of the rod D, and U/N_i. As before, U is the speed of the stirring rod and N_i is the buoyancy frequency of initial stratification.

The combined thickness of a layer and its neighbouring interfaces was measured most clearly with the plot of vertical density gradient as shown in figures 6(*b*) and 7(*b*). The vertical density gradient is a sharp peak at an interface. The distance between two adjacent peaks was defined as a *step size*, l_s, when two peaks were of similar sizes. When there were only two interfaces, they approached each other over time owing to the expansion of boundary mixed layers. In such case, the minimum distance that the adjacent peaks achieved before they vanished was considered as a step size as long as the interfaces were of the same strength. The length scale showed both temporal and spatial variations so that the minimum distance between two peaks of the same strength that did not merge was taken as the step size. In table 1, the results are listed with the external parameters, U, N_i, U/N_i, and D.

The size of the step was compared with the external length scales D and U/N_i. In table 1, there are two pairs of runs that have similar parameters except for the sizes of the rods. One pair comprised Runs 2 and 5, and the other Runs 4 and 7. The sizes of the rods, D, are increased by 75% in the first pair and 47% in the second pair, but the sizes of the steps do not change significantly. As shown in figure 12, which is the plot of U/N_i versus the step size l_s, the run with $D = 1.29$ cm, marked * in the figure, showed a larger step than the runs with $D = 3.33$ cm, which are marked o. Moreover, the runs with $D = 2.26$ cm, marked x, showed a large variation in step sizes. Thus

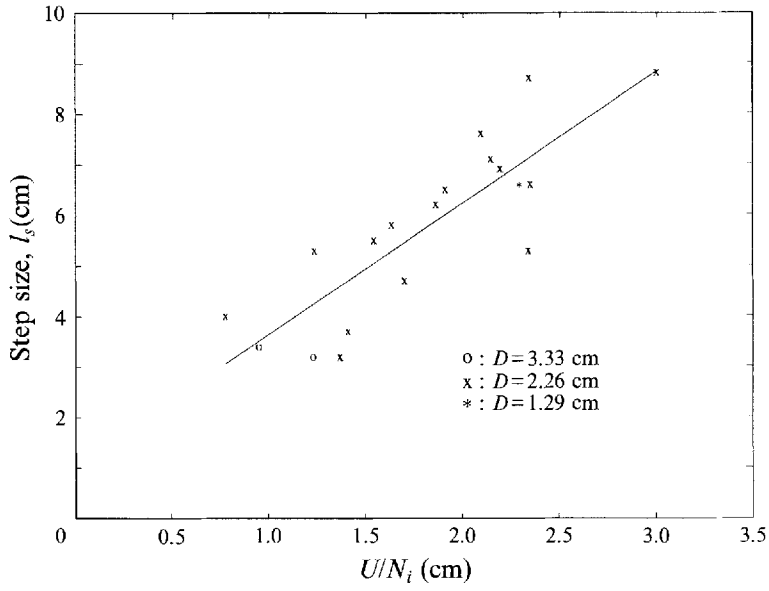

FIGURE 12. The relation between the sizes of the steps and the external length scales, D and U/N_i. The data for this figure are in table 1. The solid line is the least-square fit to the data points.

it is clear that the sizes of rods do not determine the step sizes. On the other hand, l_s and U/N_i showed a tendency toward a linear relation. The correlation coefficient between l_s and U/N_i is 0.85. In figure 12, the solid line is the least-square fit to the data and the formula is

$$l_s = 2.6\frac{U}{N_i} + 1.0\,\text{cm}. \tag{4.1}$$

As U/N_i increases, l_s inceases and becomes comparable to the depth of the tank near the stability boundary. Thus, the depth of the tank becomes a strong obstacle in observing the layering. An experiment with a deeper tank is necessary to extend the investigation of the dependence of l_s upon U/N_i down to the stability boundary.

Spectral analysis was done with the density and density gradient profile to find the length scale. The spectrum also showed the increase of step size clearly, but a single profile was not long enough to quantify the length scales. In general, the spectral analysis was less useful than the above length-scale analysis.

4.2. *Energetics*

The speed of the stirring rod was known accurately so that the work done to the test fluids, W, was estimated using a drag coefficient with the formula

$$\frac{W}{\text{one excursion}} \equiv \frac{1}{2}\bar{\rho}\, C_d\, U^2 L\, H\, D. \tag{4.2}$$

Here, H is the depth of the tank, L is the length of an excursion, $\bar{\rho}$ is the mean density of the fluid, U is the speed of the rod, D is the diameter of the rod, and C_d is drag coefficient. C_d was obtained from figure 5.11.6 in Batchelor (1967). The rod generated both internal waves of amplitude 1 cm and turbulence. Equation (4.2) is for a homogeneous fluid so it was not clear how much of the work done to the fluid was used to generate the internal waves. A few excursions were enough to supply

energy for the waves. Because the rod moved perpendicular to the density surfaces, it was not a good wave maker. Also, the wave energy could not radiate out of the tank, so the energy used to generate internal waves should be far less than that used to make turbulence. When the rod changed its direction, as one reviewer pointed out, some mixing that could not be incorporated in the equation might have occurred. However, the time for the reversal was short compared to that for an excursion. In addition, the shadowgraph did not show a significant mixing event caused by the reversal.

The total work done must be dissipated in two ways: by friction and by increasing the potential energy of the fluid, i.e. mixing the stratification. With the density profiles of about 1 mm resolution, the potential energy change of the fluid, ΔE_P, was calculated with the definition

$$\Delta E_P(t) \equiv A \int_{bottom}^{top} (\rho(z,t) - \rho_i(z))\, g\, z\, \mathrm{d}z. \tag{4.3}$$

Here, A is the area of the tank, $\rho_i(z)$ the initial density profile, and $\rho(z)$ a density profile measured at later time. The vertical integration was done using the modified Simpson's Rule. W and ΔE_P were normalized with the difference of potential energy between the initial state and the completely mixed state. With W and ΔE_P, the mixing efficiency or the flux Richardson number, R_f, is defined as

$$R_f \equiv \frac{\mathrm{d}(\Delta E_P)}{\mathrm{d}(W)}$$

$$= \frac{\text{the change of the potential energy for a certain time interval}}{\text{work done to the fluid for that time interval}}. \tag{4.4}$$

Different patterns of evolution of R_f were seen depending on Ri_o. In the non-layering case (for $Ri_o < Ri_c$), R_f monotonically decreased over time as shown in figure 13(*a*). The decrease can probably be explained by the expansion of the boundary mixed layers, since in these boundary layers there was little stratification to mix. This is also visible in the shadowgraphs taken during Run 14 (figures 5*b*, 5*c*, and 5*d* with $Ri_o < Ri_c$). The signature of active turbulent mixing is strong in the interior, but is greatly reduced in the boundary mixed layers.

In the layering case ($Ri_o > Ri_c$), R_f can be divided into three stages of evolution (see figures 13*b* and 13*c*). These are related to the three different stages of the density evolution: (i) the initiation of steps, (ii) the equilibrium state, and (iii) the two layer state. If figures 13(*b*) and 13(*c*) are compared, the first stage shows two completely different modes of R_f evolution, depending on Ri_o. For Ri_o close to Ri_c, as shown in figure 13(*b*), there is a decrease of R_f during the first stage as in the non-layering case. This decrease yields to the second stage, where R_f is rather constant. However, another pattern is seen for $Ri_o \gg Ri_c$ as shown in figure 13(*c*). R_f sharply increases during the first stage. In figure 14(*a*), the evolution of R_f during the first stage is plotted as a function of W, for fixed Re and the different values of Ri_o. As Ri_o increases, the rate of increase of R_f changes from a negative to a positive, but it is not clear why and when the transition occurs. In figure 14(*b*), the evolution of R_f of the runs with high Ri_o is plotted as a function of W All the runs clearly show the initial increase of R_f.

The second stage has a nearly constant value of R_f. The interior was in an equilibrium state; the density structure did not change much so that R_f did not change much either. In figure 13(*b*), the second stage is clear, but some runs did not

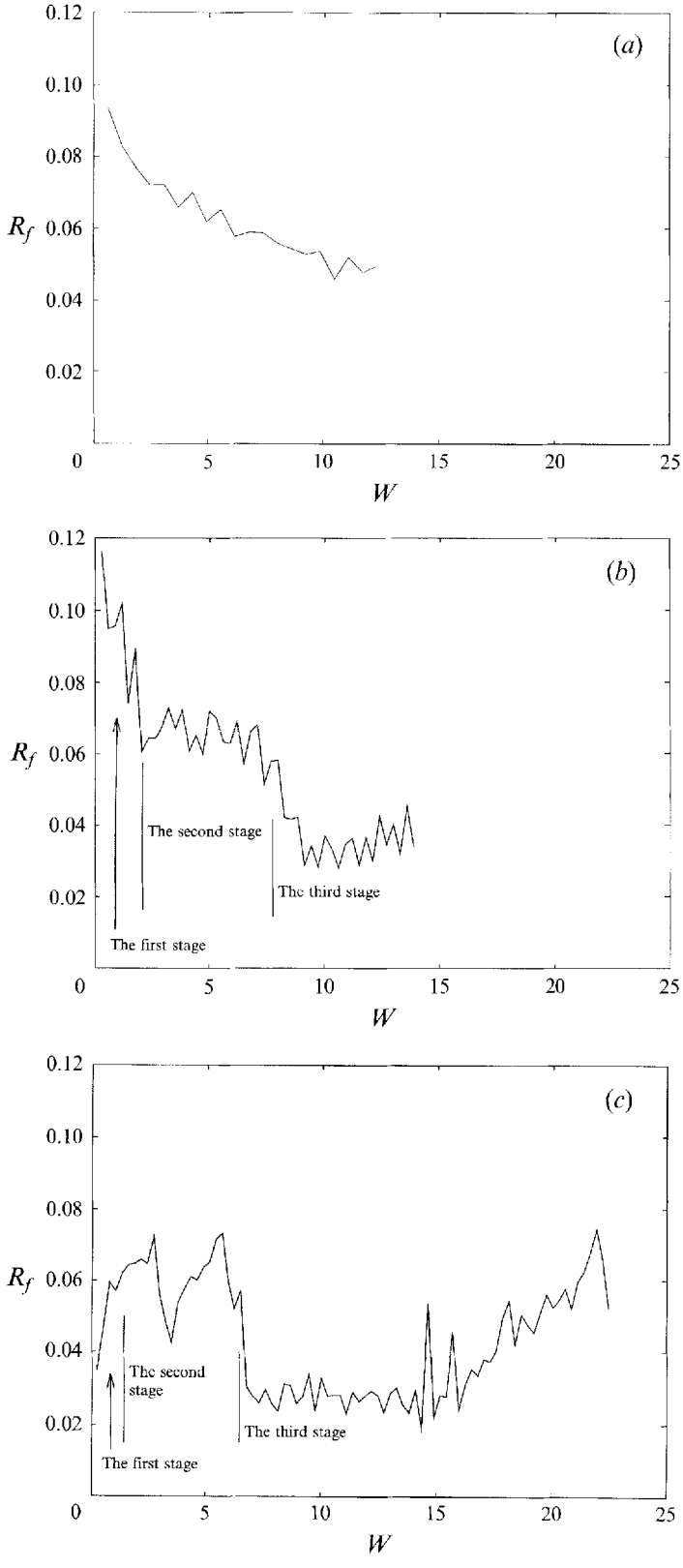

FIGURE 13 (*a–c*). For caption see facing page.

have a long enough second stage for this phenomenon to be evident. In addition, the expansion of the boundary mixed layers caused a merging or decay of interfaces, and contaminated the constancy (see figure 13*c*). The measured value of $R_f \approx 0.06$ during the second stage is low compared to those of the turbulent mixing experiments by others or estimated for oceanic turbulence. However, during the first stage, some runs showed R_f of around 0.1 (see figure 13*c*). Considering the decreasing effect of the boundary-layer expansion, R_f is not significantly different from those of the previous experiments. In addition, most of the previous turbulent mixing experiments studied only the early state of the first stage of the present experiments.

The border between the second and third stages was clear. R_f sharply decreased. Owing to the advance of the boundary mixed layers, the test fluid became two mixed layers with a strong interface, which intensified the interfacial Richardson number. A sharp decrease of R_f was observed between the border of the second and third stages. This phenomenon indirectly supports the trend that R_f decreases as Ri_o increases beyond Ri_c. During the third stage, R_f was relatively uniform compared to those of the first stage and the transition period from the second to the third stage. This phenomenon can be seen in figures 13(*b*) and 13(*c*). Eventually, the remaining interface also decayed, resulting in an increase of R_f as shown in figure 13(*c*).

The relationship between R_f and Ri is the most important assumption of the stability theory. Using the results from the third stage of Runs 17 and 18, i.e. after the fluid became two well-mixed layers, the relation between R_f and the local Richardson number Ri_l was found and presented in figure 15. The definition of Ri_l is

$$Ri_l \equiv \frac{g\Delta\rho l}{\bar{\rho}U^2}, \tag{4.5}$$

where $\Delta\rho$ is the density difference across the interface, and l is the thickness of the region in which the density gradient was larger than that of the initial state. For $1 < Ri_l < 10$, R_f decreases uniformly as Ri_l increases; for $Ri_l > 10$, R_f becomes uniform. The present experiments were not designed to find the complete relationship between R_f and Ri_l, and unfortunately the change of R_f as Ri_l decreases to zero could not be accurately determined. However, the decrease of R_f during the final interface decay, which can be seen at the very right in figure 13(*c*), implies a decrease of R_f as Ri_l approaches zero. Therefore, an increase of R_f as Ri_l increases from zero is expected but was not fully resolved. If true, the overall behaviour is in agreement with the assumption of Phillips/Posmentier as sketched in figure 1(*a*).

In § 4.1, an empirical relationship between the step size and the external parameters was found. A simple energetic argument can explain the initial increase of the step size. Assume that a linearly stratified fluid of depth H is stirred with rod at speed U and turns into a series of n completely mixed layers of depth h. To see the change in potential energy, consider that the potential energy, E_P, of a stratified unit column of

FIGURE 13. The mixing efficiency R_f versus work done W. (*a*) Run 14, $Ri_o < Ri_c$. R_f decreases monotonically to the end of the run. (*b*) Run 5, $Ri_o > Ri_c$. (*c*) Run 18, $Ri_o \gg Ri_c$. In (*b*) and (*c*), R_f shows three different stages of evolution. In (*b*) R_f decreases initially, but in (*c*) R_f increases initially. In (*b*) the second stage is clear, but in (*c*) the second stage is contaminated by the merging and decay of interfaces due to the advance of the boundary mixed layers.

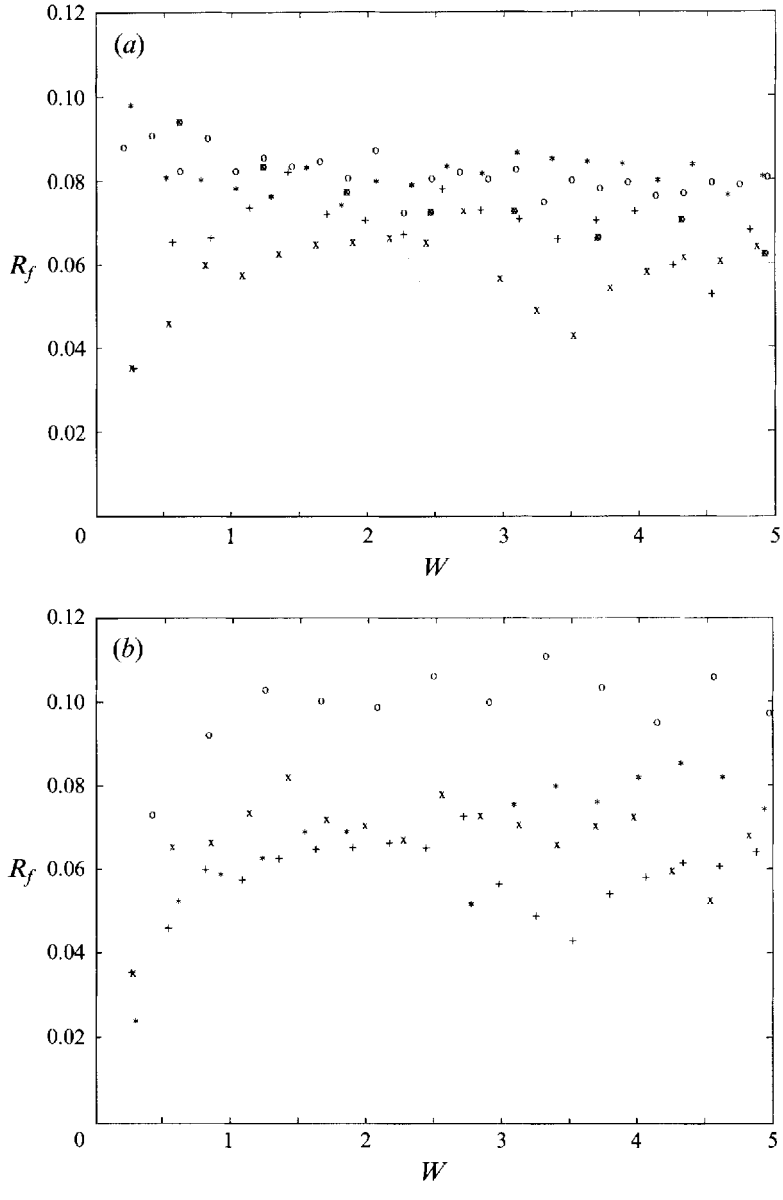

FIGURE 14. Examples of the initial change of R_f. (*a*) *Re* is fixed at 547. Ri_o is: x, 3.3 (Run 18); +, 2.2 (Run 17); o, 1.5 (Run 15); *, 1.2 (Run 16); and ⊗, 0.3 (Run 14). For $Ri_o > Ri_c$, R_f shows a decrease. However, for $Ri_o \gg Ri_c$, R_f shows a sharp initial increase. (*b*) For $Ri_o \gg Ri_c$, all show an initial increase. The values of *Re* and Ri_o of each case are: +, 547, 3.3 (Run 18); x, 547, 2.2 (Run 17); *, 730, 1.9 (Run 54); and o, 860, 1.4 (Run 58), respectively.

height h is defined as

$$E_P = \int_{-h/2}^{h/2} (\rho_o + z\frac{\partial \rho'}{\partial z}) gz \, dz. \tag{4.6}$$

Here, ρ_o is a reference density of the layer and ρ' is deviation from ρ_o. If the buoyancy frequency N is constant,

$$E_P = \tfrac{1}{2}\rho_o g h^2 - \tfrac{1}{12}\rho_o N^2 h^3, \tag{4.7}$$

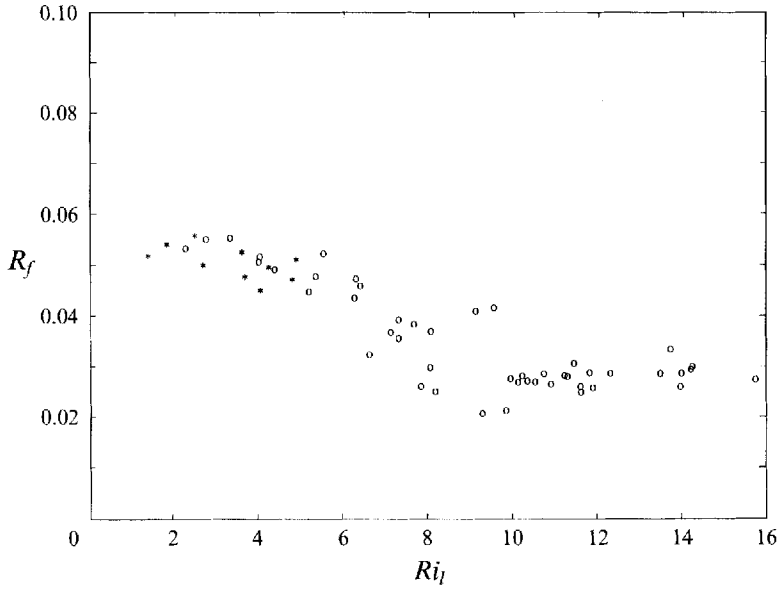

FIGURE 15. Examples of R_f versus Ri_l. The data during the third stage of Runs 17 and 18 were used. The mixing efficiency, which is equivalent to flux Richardson number R_f decreases as Ri_l increases and becomes nearly constant for $Ri_l > 10$. Here, * denotes Run 17, and o Run 18.

where $N^2 = -(g/\rho_o)(\partial\rho'/\partial z)$. The first term in the right-hand side of (4.7) is independent of N^2 and defines the potential energy of a completely mixed state. The second term, $\rho_o N^2 h^3/12$, can be considered as the change in potential energy by mixing. This vanishes with mixing, which is accomplished by setting $\partial\rho'/\partial z = 0$. Now consider a pile of n layers. Let the reference density ρ_m of each layer be

$$\rho_m = \rho_r - (n/2 - m)\, h \frac{\partial \rho}{\partial z},$$

where $\partial\rho/\partial z$ is constant. Each layer will have a potential energy as given by (4.7) with ρ_m substituted for ρ_o. If the N of an initial state is N_i = constant, then the pile is a stack of stratified layers which form a uniformly stratified fluid. If we assume that each layer is perfectly mixed, then the pile is a stack of steps. The potential energy difference between the two is found by adding up the second term of the right-hand side of (4.7) n times, so that the change in potential energy is $n\rho_o N^2 h^3/12$. Since in a fluid of depth H with n layers, $H = nh$, we may rewrite the change in potential energy ΔE_P as fluid changes from a uniformly stratified fluid to a stack of n steps as

$$\frac{\Delta E_P}{\text{unit area}} = \rho_o N_i^2 H^3/12n^2 = \rho_o N_i^2 H h^2/12. \tag{4.8}$$

If we consider $R_f = \Delta E_P/W$, then from (4.2) and (4.8), we get the relation between h and other parameters,

$$h = \left(\frac{6kLR_fC_d}{A}\right)^{1/2} D^{1/2}\, \frac{U}{N_i}. \tag{4.9}$$

Here, k is the number of excursions, and A is the area of the tank. As time progresses, k increases; consequently, so does h. From (4.1) and (4.9), $(6kLR_fC_d/A)^{1/2}D^{1/2} \approx 2.6$. If we insert the values of layer size from the experiments to find k for the equilibrium

state, we get $k \approx 100$. This value of k is far smaller than the experimental values for which layers appear. In the present experiments, there were two methods of increasing the potential energy. One was to mix the stratification locally, i.e. forming a step-like density structure; the other was to transport the density throughout the fluid column. In the experiments, the latter method and the no-flux condition at the horizontal boundaries produce the expanding boundary mixed layers. The estimation of k is crude, but we can see that the greater part of the work done to the fluid was used to expand the boundary mixed layers during the initiation of the steps.

The size of steps increases over time according to (4.9), but the data showed that the steps stopped growing and reached an equilibrium state. It is not clear when the steps reach the equilibrium state in the scope of the present experiments, but when they reach the equilibrium state, the size of step h is expected from (4.9) to be

$$h \approx D^{1/2} \frac{U}{N_i}.$$

This shows $D^{1/2}$ dependence but the present experiment does not, as shown in (4.1). Moreover, owing to the ambiguity in estimating k and R_f of the interior, the constant of proportionality could not be determined. The results are more consistent with a fixed percentage of the kinetic energy of the eddies being used to alter potential energy of the steps, but why this is so remains unsolved.

4.3. *Density flux*

The horizontal average of the mass conservation equation is

$$\frac{\partial}{\partial t}\overline{\rho}(z,t) = -\frac{\partial}{\partial z}F(z,t). \tag{4.10}$$

Here, the overbar denotes horizontal averaging, and $F(z,t)$ is the vertical density flux. Since the density flux is zero at the horizontal boundaries, vertical integration of the above equation gives

$$F(z,t) = \int_z^{top} \frac{\partial \overline{\rho}(z',t)}{\partial t}\,\mathrm{d}z'. \tag{4.11}$$

Since the density profile was measured after active turbulence decayed, the measured density profile was a horizontal average. The difference between the density profiles before and after a cycle was used for the time differentiation. For all cases where this calculation was done with recorded data, the no-flux condition at the other boundary was satisfied within a very small range of error. This shows that both the calculation and probe drift correction were accurate. In addition, the density flux calculation does not contain any ambiguous estimation, such as the estimation of work done. The vertical integral of the density flux times the gravitational acceleration, g, gives the time differentiation of potential energy change. When calculated in this way, the change was consistent with the mixing efficiency analysis, so the accuracy of the measurements and calculations was again verified. In the non-layering case, the interior density structure changed slightly as explained in § 3, so that a uniform density flux was expected in the interior. The density flux contours of a non-layering case (Run 14) are shown in figure 16. The figure does show a region of nearly uniform density flux that shrinks over time. At the horizontal boundaries, the density flux should become zero, and in the boundary mixed layers the density gradient is almost zero so flux is very small. Thus, the profile of the density flux

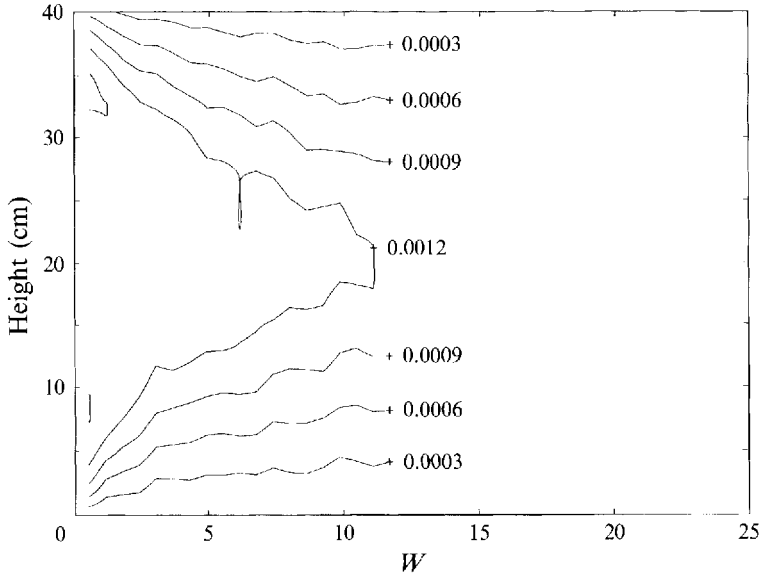

FIGURE 16. The density flux contours of Run 14 in g s^{-1}. In the interior the density flux is approximately uniform. The interior density gradient is also uniform as shown in figure 4.

has the shape of a plateau. As the boundary mixed layers expanded, the width of the plateau decreased while its height stayed nearly the same. As discussed earlier, the decreasing width probably caused the monotonic decrease of R_f as shown in figure 13(*a*).

The most prominent feature of the layering case is that the density flux was uniform in the layered interior as shown in figure 17(*a*), though the density gradient varied greatly in the interior as shown in figure 17(*b*). This supports the theory of Posmentier (1977) clearly, since the density flux of fully developed steps should be constant regardless of the density gradient. The divergence of the density flux was quite small as long as the interior structure stayed the same. This means that the density flux generated at the bottom boundary mixed layer passed through the interior all the way to the top boundary layer without changing the interior density structure. It suggests that turbulence can transport scalar properties such as heat, salt, or density further than the length scale of turbulent eddies without changing the structure of the stratification.

The merging of the interfaces resulted in a local maximum of density flux in time and space. During the merging, the thickness of the interfaces increased, and as an interface became thicker, its density gradient decreased. Turbulence became more active so that mixing was more effective since the Ri_l of the interface was larger than Ri_c. In addition, the region of density gradient expanded vertically and more of the turbulent kinetic energy was used to mix the density difference, so this also increased R_f. The increase of the density flux, F, also can be explained using the idealized relation between R_f and Ri. During the merging, Ri of the interfaces decreases so that R_f increases. At the layer between the interfaces, Ri increases locally and R_f also increases locally, since the layer has $Ri < Ri_c$. After the merging an interface with greater density difference exists so Ri of the new interface is larger than those of the old merging interfaces. Consequently R_f is lower than

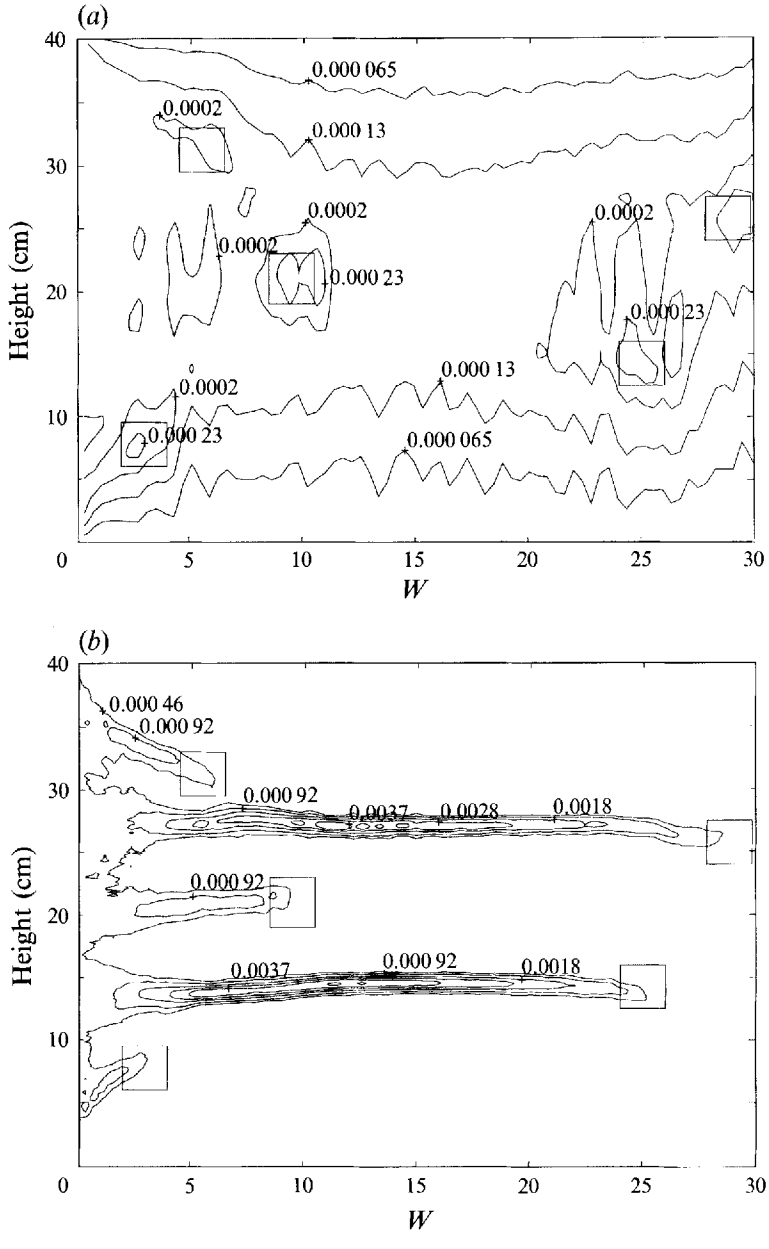

FIGURE 17. (*a*) The density flux contours of Run 2. Ri_o and Re of this run were 0.32 and 223, respectively in g s^{-1}. The small boxes in the figure are examples of the local maximum of the density flux. (*b*) The density gradient contours of the run in g cm^{-4}. The small boxes in the figure correspond to the termination of interfaces. The density flux is uniform in the layered interior, regardless of the density gradient. Every local maximum of density flux contours in (*a*) is related to the termination of the interfaces in (*b*).

the original value. Thus, the merging accompanies a local maximum in the density flux.

The decay of the interface also showed a local maximum. The small boxes in figures 17(*a*) and 17(*b*) are the examples. Every local maximum in figure 17(*a*) is

related to the termination of the interfaces in figure 17(*b*). The density gradient of a decaying interface decreased as did Ri, and the density flux increased locally in time and space. As the decay progressed, Ri of the decaying interface weakened and R_f also decreased. The decay showed a local maximum. During the decay of an interface, somewhere within the interface thereis a point where $\partial\rho/\partial t = -\partial F(z,t)/\partial z = 0$.† This means there is a spatial extremum of F. Since the magnitude of the gradient decreases

$$\frac{\partial}{\partial t}\frac{\partial \rho}{\partial z} = -\frac{\partial^2 F}{\partial z^2} > 0, \tag{4.12}$$

so the extremum is a spatial maximum.

The molecular diffusive flux and the turbulent flux are compared at the strongest interface formed during the present experiments. The molecular diffusive flux $F_d = \kappa_s \Delta\rho/d$. Here, κ_s is the molecular diffusivity of salt, $\Delta\rho$ the density difference across the interface, and d the thickness of the interface. In the present experiments the maximum value of $\Delta\rho = 0.066\,\mathrm{g\ cm^{-3}}$, $d = 2\,\mathrm{cm}$, and $\kappa_s = 1.5 \times 10^{-5}\,\mathrm{cm^2\ s^{-1}}$. So, F_d was about $1 \times 10^{-4}\,\mathrm{g\ s^{-1}}$. The turbulent density flux was more than $1 \times 10^{-3}\,\mathrm{g\ s^{-1}}$, which was 10 times larger than the molecular diffusive flux. Since at the strongest interface the turbulent flux dominated, it is probable that the turbulent flux dominates even more strongly for other cases that have weaker interfaces.

5. Conclusions

Linearly stratified fluids were mixed with rods that were moved horizontally at constant speeds. In most cases, the fluids were stirred until they were completely mixed, so the evolution of the density structures and the related energetics could be studied. With high-resolution density profiles, the evolution of the density structure was observed clearly.

The fluids could be divided into boundary layers and an interior. The boundary layers expanded into the interior over time owing to the no-flux condition at the horizontal boundaries. The interior, whose density gradient was initially uniform, evolved into steps when the overall Richardson number, Ri_o, was large and the Reynolds number of the rod, Re, was small. By changing Re and Ri_o, the stability boundary of the layer formation was found. As the instability theory of Phillips/Posmentier predicted, the layering occurred when Ri_o was larger than a critical value Ri_c, which forms the stability curve. Ri_c increases exponentially as Re increases.

The interior steps also showed evolution. Small steps formed first, and they became larger through the merging and decay of the interfaces. The merging occurred between two closely spaced interfaces. This implies that there might be a minimum step size but the present experiments cannot verify this idea. The interior seemed to reach an *equilibrium* state where the interior structure did not change except for the merging caused by the expansion of the boundary mixed layers. The size of the equilibrium steps, l_s, is found to be a linear function of the external length scale U/N_i. It is interesting that the size of the step was independent of the size of the stirring rods within the scope of the present experiments. In Ruddick *et al.* (1989), a stratified fluid was mixed with a sinusoidal stirrer and the maximum of U/N_i was about 1 cm. Considering that the average of U/N_i over a sinusoidal cycle would be a little less, our empirical relation predicts scales of order 2 cm, which agrees with their observation.

† In figure 1(*b*), the density does not change over time at the point A.

The energetics showed that the evolution of R_f was closely related to the evolution of the density structure. While the non-layering case (for $Ri_o < Ri_c$) showed a monotonic decrease of R_f throughout a run, the layering case (for $Ri_o > Ri_c$) showed three different stages of R_f evolution in relation to the evolution of the steps. During the initiation of the steps, depending on the value of Ri_o, R_f showed two completely different modes of time change: a decrease of R_f for Ri_o close to Ri_c, and a sharp increase for $Ri_o \gg Ri_c$. To clarify the evolution of R_f during the stage, an experiment with a constant boundary flux or a deep tank is necessary. When the steps reached an equilibrium state, R_f became uniform regardless of the initial behaviour as long as the interior steps were maintained. As the fluid became two mixed layers, R_f decreased sharply, then it became uniform again. During the equilibrium state, the density flux was uniform throughout the layered interior regardless of the interior density gradient; this phenomenon is consistent with the prediction of Posmentier (1977).

According to Posmentier (1977), R_f of the equilibrium state should be less than that of the initial states, although the change of R_f during the development of the steps does not have to be monotonic. It is not clear whether the smaller R_f of the equilibrium state verifies the prediction of the theory, or whether it is due to the expansion of the boundary mixed layers. For $Ri_o \gg Ri_c$, R_f of the equilibrium state is higher than that of the initial state; this phenomenon seems to contradict Posmentier (1977). The initial increase is, however, in agreement with Turner (1973), who discussed the energetics of layering in the presence of turbulence. Initially, stratification is so large that turbulence cannot mix the stratification effectively. By developing a step-like density structure, the local gradient Richardson number is reduced to a value at which turbulent mixing can be maintained. One consequence of this discussion is that during the formation of steps more mixing is allowed in the layers so that the mixing efficiency increases; this phenomenon was observed with the runs of $Ri_o \gg Ri_c$.

A relation between R_f and the local Richardson number based on the thickness of an interface, Ri_l, was found. There was a uniform decrease of R_f as Ri_l increases for $1 < Ri_l < 10$. This relation is consistent with the assumption used by Phillips/Posmentier. For $Ri_l > 10$, R_f becomes uniform. This was not observed in the previous turbulent mixing experiments such as those by Linden (1979) and Ivey & Imberger (1991).

The present experiments show that uniform turbulent mixing can also generate step-like density structures. In addition, mixing does not have to be localized to make a step. Quantitatively, we find that it takes many mixing events to produce a mixed layer: for example, the layers in figures in 7, 8, 10 and 11 were found after hundreds or thousands of excursions. The conditions under which layering occurs may be of interest to oceanographers. For instance, the presence of oceanic layers means that the oceanic Ri_o is larger than Ri_c. In addition, according to these results, a mixed layer in the oceans may require hundreds of mixing events, rather than one gigantic event.

These experiments were relatively easy to do, but they required the careful maintenance of a constant room temperature and extremely uniform stirring. They showed how layers emerged in a system that was subjected to numerous turbulent events. The results did not appear to require a detailed knowledge of small-scale mechanisms. The results presented in this paper suggest that the density structure within a mixed layer of fluid may reflect the temporal history of the mixing, and not just the structure of the mixing instability.

There are still many questions that are unanswered. We find the following especially interesting.

1. Is there a minimum equilibrium step size?
2. What determines the initial step size?
3. What are the effects of molecular diffusion?
4. How can we apply the results to mixing in geophysical problems?

We thank Dr Karl Helfrich for comments and generously lending us the equipment. Robert Frazel helped us in the laboratory. The early evolution of this work benefited from discussions with Jay Portnow. Research was supported by the Ocean Sciences Division of the National Science Foundation under grant OCE89-15408. Young-Gyu Park was partly supported by Korean Government Overseas Scholarship Grants. Woods Hole Oceanographic Institution contribution number 8130.

Appendix A. Parameters of the experiments

Run number	U (cm s^{-1})	D (cm)	Re	N_i^2 (s^{-2})	Ri_o	Number of cycles	Excursions per cycle
1	1.0	1.29	129	0.52	0.87	32	250
2	1.7	1.29	223	0.55	0.32	80	100
3	3.0	1.29	387	0.60	0.11	22	50
4	1.0	2.26	226	0.53	2.71	72	100
5	1.7	2.26	390	0.60	1.06	47	50
6	3.0	2.26	678	0.54	0.31	20	30
7	1.0	3.33	333	0.66	7.32	33	50
8	1.5	3.33	496	0.60	2.96	24	30
9	1.6	3.33	390	2.83	12.96	15	100
10	2.77	2.26	626	3.86	2.57	50	100
11	1.73	2.26	391	4.88	8.33	54	150
12	2.42	2.26	547	0.60	0.52	20	50
13	2.42	2.26	547	1.19	1.04	50	50
14	2.42	2.26	547	0.35	0.31	20	30
15	2.42	2.26	547	0.69	1.47	75	50
16	2.42	2.26	547	1.34	1.17	65	50
17	2.42	2.26	547	2.46	2.15	57	100
18	2.42	2.26	547	3.83	3.34	83	150
19	2.02	2.26	457	1.41	1.76	42	100
20	2.23	2.26	504	0.86	0.88	50	50
21	2.02	2.26	456	0.89	1.11	50	50
22	2.02	2.26	456	1.12	1.40	20	50
23	2.02	2.26	456	0.74	0.93	49	50
24	2.02	2.26	456	0.56	0.70	45	50
25	2.21	2.26	500	0.56	0.59	65	30
26	1.67	2.26	379	0.31	0.57	37	50
27	2.71	2.26	612	0.30	0.21	15	50
28	1.26	2.26	285	0.29	0.93	45	70
29	2.02	2.26	456	0.42	0.53	50	30
30	2.89	2.26	653	3.42	2.09	120	30
31	2.23	2.26	504	0.30	0.31	30	30
32	2.02	2.26	456	0.27	0.34	30	30
33	2.79	2.26	631	1.40	0.92	65	30
34	2.79	2.26	631	1.69	1.11	70	40
35	2.23	2.26	504	0.24	0.25	20	30

Run number	U (cm s^{-1})	D (cm)	Re	N_i^2 (s^{-2})	Ri_o	Number of cycles	Excursions per cycle
36	2.62	2.26	592	1.62	1.21	60	50
37	2.79	2.26	631	1.08	0.71	50	30
38	3.24	2.26	732	1.37	0.67	50	30
39	1.90	2.26	429	0.27	0.38	35	30
40	3.23	2.26	730	1.10	0.54	40	30
41	2.62	2.26	592	1.14	0.85	38	50
42	3.24	2.26	732	0.83	0.40	35	30
43	2.42	2.26	547	0.95	0.83	40	50
44	4.29	2.26	970	0.79	0.22	32	20
45	3.24	2.26	732	2.39	1.16	55	50
46	4.29	2.26	970	1.05	0.29	28	30
47	4.29	2.26	970	2.56	0.71	24	50
48	3.80	2.26	859	1.12	0.40	35	40
49	2.79	2.26	631	0.84	0.73	50	30
50	4.29	2.26	970	1.57	0.44	35	30
51	1.72	2.26	389	0.14	0.24	21	40
52	4.29	2.26	970	4.31	1.20	30	70
53	4.29	2.26	970	2.10	0.58	22	50
54	3.24	2.26	732	3.93	1.91	45	100
55	3.24	2.26	732	3.03	1.47	45	70
56	4.29	2.26	970	2.84	0.79	35	50
57	3.80	2.26	859	3.16	1.12	35	70
58	3.80	2.26	859	4.02	1.42	30	100
59	3.80	2.26	859	1.59	0.56	18	30
60	3.80	2.26	859	2.53	0.89	40	50
61	3.80	2.26	859	2.04	0.72	40	40
62	2.79	2.26	631	0.54	0.35	30	30
63	5.55	2.26	1254	1.60	0.27	20	25
64	5.55	2.26	1254	4.10	0.68	15	100
65	6.37	2.26	1440	1.66	0.21	25	25
66	6.37	2.26	1440	2.14	0.27	20	40
67	6.37	2.26	1440	3.89	0.49	15	80
68	5.55	2.26	1254	2.18	0.36	22	40
69	6.37	2.26	1440	2.59	0.33	22	40
70	5.55	2.26	1254	3.14	0.52	20	60
71	5.55	2.26	1254	2.57	0.43	20	50
72	6.37	2.26	1440	3.15	0.40	18	60
73	7.11	2.26	1607	4.11	0.42	10	80
74	7.11	2.26	1607	3.08	0.31	16	60
75	2.79	2.26	631	0.45	0.30	22	30
76	2.42	2.26	547	1.07	0.93	29	100

REFERENCES

BATCHELOR, G. K. 1967 *An Introduction to Fluid Dynamics*. Cambridge University Press.

GIBSON, C. H. 1980 Fossil temperature, salinity and vorticity turbulence in the ocean. In *Marine Turbulence* (ed. J. C. Nihoul), pp. 221–257. Elsevier.

GIBSON, C. H. 1982 Alternative interpretations for microstructure patches in the thermocline. *J. Phys. Oceanogr.* **12**, 374–383.

GIBSON, C. H. 1986 Internal waves, fossil turbulence, and composite ocean microstructure spectra. *J. Fluid Mech.* **168**, 89–117.

GIBSON, C. H. 1987*a* Oceanic turbulence: big bangs and continuous creation. *J. Physiochem. Hydrodyn.* **8**, 1–22.

GIBSON, C. H. 1987*b* Fossil turbulence and intermittency in sampling oceanic mixing processes. *J. Geophys. Res.* **92**, 5383–5404.

GREGG, M. C. 1989 Scaling turbulent dissipation in the thermocline. *J. Geophys. Res.* **94**, 9686–9698.

GREGG, M. C. 1991 A study of mixing in the ocean: a brief history. *Oceanography* **4**, 39–45.

HOGG, N. G., BISCAYE, P., GARDNER, W. & SCHMITZ, W. J. JR 1982 On the transport and modification of the Antarctic Bottom Water in the Vema Channel. *J. Mar. Res.* **40** (Suppl.), 231–263.

IVEY, G. N. & CORCOS, G. M 1982 Boundary mixing in a stratified fluid. *J. Fluid Mech.* **121**, 1–26.

IVEY, G. N. & IMBERGER, J. 1991 On the nature turbulence in a stratified fluid. Part I: The energetics of mixing. *J. Phys. Oceanogr.* **21**, 650–658.

LINDEN, P. F. 1979 Mixing in stratified fluids. *Geophys. Astrophys. Fluid Dyn.* **13**, 3–23.

LINDEN, P. F. 1980 Mixing across a density interface produced by grid turbulence. *J. Fluid Mech.* **100**, 691–703.

MUNK, W. H. 1966 Abyssal Recipes. *Deep-Sea Res.* **13**, 707–730.

OSBORN, T. R. & COX, C. S. 1972 Oceanic fine structure. *Geophys. Fluid Dyn.* **3**, 321–345.

PHILLIPS, O. M. 1972 Turbulence in a strongly stratified fluid - Is it unstable? *Deep-Sea Res.* **19**, 79–81.

POSMENTIER, E. S. 1977 The generation of salinity finestructure by vertical diffusion. *J. Phys. Oceanogr.* **7**, 292–300.

RUDDICK, B. R., MCDOUGALL, T. J. & TURNER, J. S. 1989 The formation of layers in a uniformly stirred density gradient. *Deep-Sea Res.* **36**, 597–609.

SCHMITT, R. W., TOOLE, J. M., KOEHLER, R. L., MELLINGER, E. C. & DOHERTY, K. W. 1988 The development of a fine- and microstructure profiler. *J. Atmos. Ocean. Tech.* **5**, 484–500.

THORPE, S. A. 1982 On the layers produced by rapidly oscillating a vertical grid in a uniformly stratified fluid. *J. Fluid Mech.* **124**, 391–409.

TURNER, J. S. 1968 The influence of molecular diffusivity on turbulent entrainment across a density interface. *J. Fluid Mech.* **33**, 639–656.

TURNER, J. S. 1973 *Buoyancy Effects in Fluids.* Cambridge University Press.

WHITEHEAD, J. A. JR & WORTHINGTON, L. V. 1982 The flux and mixing rates of Antarctic Bottom Water within the North Atlantic. *J. Geophys. Res.* **87**, 7903–7924.